Forest Ecology and Management 583 (2025) 122582

Contents lists available at ScienceDirect

Forest Ecology and Management

journal homepage: www.elsevier.com/locate/foreco

Forest temperature buffering in pure and mixed stands: A high-resolution temporal analysis with generalized additive models

Matthias Steinparzer [a,f], Loïc Gillerot [b], Boris Rewald [c], Douglas L. Godbold [a,c], Daniela Haluza [d], Qiwen Guo [a], Sonja Vospernik [e,*]

[a] Institute of Forest Ecology, Department of Forest and Soil Sciences, University of Natural Resources and Life Sciences Vienna (BOKU), Peter-Jordan Straße 82, Vienna 1190, Austria
[b] Forest & Nature Lab, Department of Environment, Faculty of Bioscience Engineering, Ghent University, Geraardsbergsesteenweg 267, Gontrode 9090, Belgium
[c] Department of Forest Protection and Wildlife Management, Mendel University in Brno Zemědělská 3, Brno 613 00, Czech Republic
[d] Department for Environmental Health, Center for Public Health, Medical University of Vienna, Kinderspitalgasse 15, Vienna 1090, Austria
[e] Institute of Forest Growth, Department of Forest and Soil Sciences, University of Natural Resources and Life Sciences Vienna (BOKU), Peter-Jordan Straße 82, Vienna 1190, Austria
[f] Environment Agency Austria, Ecosystem Research and Environmental Information Management, Spittelauer Lände 5, Vienna 1090, Austria

ARTICLE INFO

Keywords:
Forest microclimate
Temperature offset
GAM
Microclimate modeling
Tree diversity

ABSTRACT

Forests foster buffered microclimates, but causal mechanisms have rarely been studied on longer timescales and in differently diverse stands. Here, we explore temperature regulation by a young experimental forest in Austria, focusing on four common colline broadleaf species (*Acer platanoides* L., *Tilia cordata* Mill., *Quercus robur* L., *Carpinus betulus* L.) in monocultures, two- and four-species mixed stands. Air temperature was monitored in 28 forest plots for two years and compared to open-field controls. Using generalized additive models (GAMs), we investigated direct temperature offsets and lags between open-field and sub-canopy temperatures, considering diurnal and seasonal changes, and causal factors such as global mean radiation, relative air humidity, wind, and leaf area index (LAI). Forests generally had a cooling effect during the summer and a warming effect in winter, where the cooling magnitude varied with species composition and environmental conditions. Specifically, *Acer platanoides* and *Carpinus betulus* demonstrated the highest cooling capacities, and *Quercus robur* the lowest. Mixed species stands exhibited higher temperature buffering effects relative to monospecific stands, suggesting that species diversity in forests can increase the ability to regulate microclimates. Solar radiation, relative air humidity, wind speed, and LAI all significantly influenced offsets. These findings are crucial for urban forestry and environmental planning, suggesting that careful selection of tree species can optimize temperature regulation, thereby improving human thermal comfort and ecosystem processes alike.

1. Introduction

Forests substantially influence local thermal environments, creating microclimates distinct from the surrounding macroclimate (Chen et al., 1999; Geiger et al., 2009; De Frenne et al., 2019, 2021; Gillerot et al., 2024b). These microclimates feature lower daytime temperature maxima and higher nighttime minima (Chen et al., 1999; D'Odorico et al., 2013; De Frenne et al., 2019, 2021), with a global average reduction of 4.1 °C in daily maxima and an increase of 1.1 °C in minima (De Frenne et al., 2019). Buffering magnitude and patterns vary diurnally, seasonally, and interannually (Ewers and Banks-Leite, 2013; De Frenne et al., 2021; Meili et al., 2021). Warmer seasons relate to larger reductions in temperature maxima because of both higher evapotranspiration and the full leaf flushing of deciduous species - at least in temperate biomes (Wang et al., 2021). European forests, for example, reduce summer temperatures by 2.1 °C on average and increase winter temperatures by 2.0 °C (Haesen et al., 2021). During temperature extremes, such as heatwaves, forests' buffering capacity becomes critical, reducing seasonal and interannual variability mitigating impacts on biodiversity and human well-being (Renaud and Rebetez, 2009; De Frenne et al., 2021; Gillerot et al., 2022, 2024a).

This temperature buffering has not only significant implications for biodiversity and human health, but also for ecosystems. The buffering helps regulate the ecological balance in understory plant communities

* Corresponding author.
E-mail address: sonja.vospernik@boku.ac.at (S. Vospernik).

https://doi.org/10.1016/j.foreco.2025.122582
Received 3 November 2024; Received in revised form 10 January 2025; Accepted 17 February 2025
Available online 25 February 2025

by mitigating thermophilization (Royer et al., 2011; De Frenne et al., 2013; Zellweger et al., 2020) and climate change impacts, especially in forests with dense canopies (Sanczuk et al., 2023). The buffering effect of forest canopies also alleviates thermal stress, benefiting human health (Gillerot et al., 2022, 2024a).

Forest microclimates are the result of a complex interplay of meteorological factors (air temperature, precipitation, solar radiation, cloud cover, wind speed and direction, air humidity, evapotranspiration) and local conditions (topography, soil type, land cover) (Bramer et al., 2018). Trees and vegetation alter wind patterns, provide shade and elevate air humidity through transpiration and evaporation (Aussenac, 2000; Geiger et al., 2009). Leaf area index (LAI), crown structure (Kotzen, 2003; Shahidan et al., 2010), and canopy closure are influenced by species composition and affect the reflection, absorption and transmission of solar radiation, thus moderating temperature extremes (Chen et al., 1999; Zellweger et al., 2019) and temperature variations (Aussenac, 2000; Bramer et al., 2018). Dense canopies further reduce turbulent air mixing (Raupach et al., 1996; Hardwick et al., 2015), lowering wind speeds by up to a factor of 5 compared to open-fields (Davies-Colley et al., 2000; Gillerot et al., 2022). As a result, forest stand structure - particularly basal area, LAI, canopy closure and -height of overstorey trees, is thus of major importance in determining microclimates (Hardwick et al., 2015; Greiser et al., 2018; Jucker et al., 2018; Zellweger et al., 2019; Gillerot et al., 2022, 2024b). However, below-canopy structural variables might also partially determine microclimatic variation (Kovács et al., 2017).

Species composition shapes both canopy and structural properties of forest stands. For instance, deciduous and evergreen-deciduous forests in Switzerland exhibit more pronounced summer and daytime cooling than pine-dominated stands (Renaud and Rebetez, 2009; Renaud et al., 2011). Although these cooling effects are likely driven by functional traits (e.g. shade-casting ability, crown shape, leaf size, leaf shape and colour) (Zellweger et al., 2019; Rahman et al., 2020), a global meta-analysis found no consistent relationship at the global scale (De Frenne et al., 2019). In the light of the ongoing transition of temperate forests towards mixed stands to mitigate climate change effects (Morin et al., 2011; Liang et al., 2016; Ammer, 2019), tree species diversity has been hypothesized to further enhance temperature buffering (Gillerot et al., 2022; Zhang et al., 2022; Schnabel et al., 2024). This is partly, because diversity can foster increased structural complexity through spatial complementarity in aboveground biomass, leading to more complete canopy space filling (Pretzsch, 2014; Pretzsch and Schütze, 2016; Pretzsch et al., 2016). Increased vertical stratification and crown plasticity in mixed stands (Jucker et al., 2015) contribute to these effects. Despite these insights, evidence of diversity effects on thermal buffering remains mixed. Some studies indicate that tree species diversity, along with denser and more complex canopies, consistently improves temperature regulation (Wang et al., 2021; Schnabel et al., 2024). In young forest plantations, however, microclimate cooling appears to depend strongly on species identity and to a lesser degree on tree species diversity (Zhang et al., 2022). Mixture effects can be negative if interspecific competition reduces overall leaf area (Zhang et al., 2022). Mechanisms driving enhanced cooling in mixed stands resemble those that increase productivity (Zhang et al., 2022). Complementary species traits allow a more efficient use of resources such as light, water, nutrients increasing the growth of roots, stem and leaves (Pretzsch et al., 2016; Ehbrecht et al., 2017; del Río et al., 2021; Urgoiti et al., 2022; Zhang et al., 2022). A larger leaf area intensifies shading and evapotranspiration, thereby strengthening thermal buffering. Moreover, these benefits may become more pronounced as forests mature (Gillerot et al., 2022; Lindenmayer et al., 2022).

The present study aims for an in-depth analysis of the effects of species identity and diversity on subcanopy air temperature, particularly focusing on temperature offsets between forest and open-field environments. Central to our analysis are the temporal patterns - both diurnal and seasonal - alongside a suite of causal factors including global mean radiation, relative air humidity, wind speed, and LAI. Generalized Additive Models (GAMs), as conceptualized by Hastie and Tibshirani (1986) and expanded by Wood (2017), provide a methodologically sound framework for this comprehensive analysis. GAMs are recognized for their ability to accurately model smooth, non-linear relationships within time series data, a feature that has garnered appreciation within ecological modeling (Simpson, 2018; Pedersen et al., 2019; Vospernik, 2021), and in particular for modeling temperature (Guan et al., 2009; Laanaya et al., 2017). A comparison of different methods (linear regression, residuals regression, logistic regression, GAM), indicated GAMs were the best among the four models for water temperature modelling based on RMSE, bias, Nash-Sutcliffe coefficient of efficiency. Similarly, Zellweger et al. (2019) found a GAM mixed approach to model temperature buffering more efficient than generalized mixed models but did fully make use of the potential of GAMs to include and predict seasonal patterns. This analytical approach allows for an intricate examination of how temperature buffering is influenced by both temporal patterns and environmental drivers across monocultures and mixtures of four widespread broadleaf species: Small-leaved lime (*Tilia cordata* Mill.), Norway maple (*Acer platanoides* L.), common hornbeam (*Carpinus betulus* L.), and pedunculate oak (*Quercus robur* L.). Over two years of hourly resolved data are analyzed to discern the multifaceted effects of these factors, utilizing the flexibility of GAMs in capturing the complexity of ecological interactions.

We tested the following hypotheses: (i) The temperature inside a young forest significantly differs from the temperature in the open-field, indicating a substantial temperature buffering effect of young forests. (ii) There is a significant diurnal or seasonal temperature buffering between the young forest and the open-field, implying that the temperature patterns differ over time for both environments. (iii) Environmental macroclimatic factors such as solar radiation, wind speed and relative air humidity significantly affect the temperature buffering capabilities of the young forest. (iv) There are measurable microclimatic offsets between different forest plots with varying tree species compositions and LAI, suggesting variability in the temperature buffering effect throughout the young forest.

2. Material and methods

2.1. Study area

This research was conducted at the B-Tree experimental forest in Tulln an der Donau (48.317531 N, 16.066908 E) in the eastern part of Austria. B-Tree belongs to the global TreeDivNet platform, a network dedicated to tree biodiversity investigations (Verheyen et al., 2016). Established in 2013, the B-Tree site spans c. 1.2 ha and was densely planted in a gapless configuration with c. 12,000 2-year-old trees from four different broadleaf tree species, namely *Acer platanoides* L. (Ap), *Tilia cordata* Mill. (Tc), *Quercus robur* L. (Qr), and *Carpinus betulus* L. (Cb), using a hexagonal planting design with 1 m distance between trees. Prior to its transformation in 2012, the area was used as a grassland and covered sparsely with shrubs and trees. Its surroundings consist primarily of agricultural land.

The site comprises both monocultures and mixtures. Monocultures constitute four plot types (Ap, Tc, Qr, Cb), two-species mixtures two plot types (Ap and Tc – ApTc, and Qr and Cb – QrCb), while four-species plots contain all species (All) as the seventh plot type (Fig. 1). Each of the 7 plot types / species compositions is four-times replicated. In two-species plots, each species accounts for half of the total stem number, while in the four-species plots, each species makes up a quarter of the total trees. Individual species plots measure 131 m^2, while two and four-species plots are 313 m^2 (Fig. 1). Areas in between these plots were filled with species of neighboring plots, ensuring a continuously closed forest canopy. At the start of the study, in August 2020, average tree heights were: *A. platanoides* 5.5 ± 1.6 m, *T. cordata* 3.6 ± 1.2 m, *Q. robur* 4.2 ± 1.1 m, and *C. betulus* 4.1 ± 1.0 m.

Fig. 1. Aerial overview of the plot arrangement of the TreeDivNet experimental site B-Tree, Austria. The four present species (*Acer platanoides* L. (**Ap**), *Tilia cordata* Mill. (**Tc**), *Quercus robur* L. (**Qr**), *Carpinus betulus* L. (**Cb**)) are replicated as monocultures, two-species mixtures **ApTc** and **QrCb** and as four-species mixtures **All**. The plot abbreviations with a consecutive number (1–4 corresponds to the replication number) mark the sampled plots (e.g., **Ap1**, **Tc1**, …).

The site's local climate yields an average annual precipitation of 597 mm and a mean annual temperature of 9.5 °C (ZAMG, 2002). During the experimental period the average air temperature was recorded at 11.3 ± 8.4 °C, and mean wind speed and mean relative air humidity were 3.3 ± 2.6 m s^{-1}, and 73 ± 12.9 %, respectively. Mean solar radiation was 139.3 ± 224.9 W m^{-2} and cumulative precipitation 663.6 ± 0.6 mm (Table 1).

The soil at the experimental site is classified as moist chernozem, characterized by its hydromorphic properties, rich humus content, and the presence of free calcium carbonate derived from Danube River sediments.

Table 1
Climatic data of the GeoSphere weather station, close to the B-Tree study site, Austria, between 2020 and 2022.

year	air temperature [°C]	windspeed [m s^{-1}]	relative air humidity [%]	solar radiation [W m^{-2}]	cumulative precipitation [mm]
			Mean ± SD		
2020	11.4 ± 8.1	3.3 ± 2.6	74.3 ± 19.1	133.1 ± 216.7	814.4 ± 0.6
2021	10.8 ± 8.6	3.4 ± 2.5	74.4 ± 17.5	139.8 ± 223.3	630.6 ± 0.6
2022	11.9 ± 8.5	3.4 ± 2.6	71.8 ± 20.0	145.0 ± 234.6	545.8 ± 0.5

2.2. Leaf area sampling, micro- and macroclimatic measurements and phenology

The LAI was sampled according to the method described in Steinparzer et al. (2022), starting from summer 2020 until the shedding of the last marcescent leaves in spring 2023. In brief, a total of 128 leaf litter traps were deployed to collect leaf litter, which was subsequently dried, sorted by species, and weighed. Leaf biomass was then multiplied by the specific leaf area to calculate the LAI. Absolute and relative LAI, i.e. the proportional share of the tree species LAI compared to the absolute LAI in percent, were determined at plot and/or species levels. Statistical tests were carried out in R, using the packages *stats* (R Core Team, 2024) and *car* (Fox and Weisberg, 2019). One-way ANOVAs ($p < 0.05$) were conducted for all stands (Ap, Tc, Qr, Cb, ApTc, QrCb, All). Pairwise comparisons were assessed via Tukey's HSD ($p < 0.05$). Residuals met normality (Shapiro-Wilk, $p < 0.05$), and homogeneity of variances was confirmed (Levene, $p < 0.05$). No violations of these assumptions were found.

Thermochron iButtons (DS1922L; Maxim Integrated, San Jose, California, USA) were used to record ambient air temperatures beneath the canopy of every replicated plot (Fig. 1) and in the open-field adjacent to the site. The micro sensors have an accuracy of ± 0.5 °C reported by the manufacturer — a figure validated by Staines et al. (2022) with an observed accuracy of ± 0.47 °C and precision of ± 0.17 °C. To avoid edge effects, the sensors were centered in each of the 28 forest plots and placed in equal distance from the surrounding trees. In mixed forest stands, we ensured that the distribution of surrounding tree species reflected the intended proportionality of species. Under the forest canopy, the sensors were suspended at 1.1 m above the forest floor, which is the mean center of gravity of a standing adult (ISO, 1998; Johansson et al., 2014). The sensors were placed in a thin plastic bag with silica gel, as a precaution against damage by moisture (Roznik and Alford, 2012) and shielded against solar radiation (Supplementary Fig. A.1 B, C). In the open-field, three sensors were likewise positioned at 1.1 m, using wooden posts as substitutes for the trees to ensure the same suspension height and setup. The open-field sensors were placed 30 m from the southern border of the forested site (Fig. 1) to avoid interactions. Given the sensor's reliance on an internal non-rechargeable battery, we implemented a synchronised logging interval of three hours to sustain the sampling period. Sensors were cross calibrated before being installed in the plots.

The microclimatic temperature recordings continued from 6th August 2020 to 20th September 2022. The loggers were retrieved two times (1st time: from 25th February 2021 till 9th April 2021, 2nd time: from 3rd October 2021 till 16th October 2021) for data collection. To match hourly macroclimatic meteorological data (see below) with the microclimatic data from the sensors, temperature between the 180-minute logging intervals were linearly interpolated using the R *padr* package (Thoen, 2022). We did not apply gap filling to the periods where the loggers were retrieved from the field. The iButton data was screened for outliers and these were removed from the temperature time series before analysis. Time series data was adjusted to UTC local time. The same statistical tests as for LAI were applied to the mean forest temperature and mean temperature offset for each season and no violations of the assumptions were found.

Macroclimatic data, spanning from 6th August 2020 to 21st September 2022, was retrieved from a neighboring weather station in 3.84 km distance to the study site (GeoSphere weather station Langenlebarn [48.323891, 16.118055], 175 m above sea level, synoptic observation station coding: 4081 (GeoSphere Austria, 2023). These hourly macroclimatic data from the weather station were joined with the iButton data: Wind speed [m s^{-1}], relative air humidity [%], incoming solar radiation [W m^{-2}], precipitation [mm], sun hours [h], soil temperature in 20 cm soil depth [°C] and calculated ASCE-EWRI

reference (alfalfa) evapotranspiration ETo [mm h^{-1}] from the R GitHub package gowusu/sebkc (Owusu, 2023). Precipitation, sun hours, soil temperature in 20 cm soil depth and ETc were subsequently not used due to possible multi-day lag, coarse data resolution or stark collinearity with temperature, wind speed, solar radiation, and relative air humidity (data not shown).

During the LAI sampling periods, phenological events such as bud break, leaf flushing until the canopy was fully developed, the start of leaf shedding, and the end of leaf shedding were documented (ZAMG, 2019; Supplementary Table A.1). For analysis, we selected cardinal points (Supplementary Table A.1, Fig. 3 A-J) to represent both in situ phenological observations and established meteorological dates (e.g., A (DOY 60) for meteorological spring, B (DOY 80) for calendrical spring, F (DOY 172) for summer solstice, and J (DOY 355) for winter solstice). Across years, bud break typically occurred between C (DOY 90) and D (DOY 120), with *A. platanoides* and *C. betulus* initiating first (often around DOY 90–95), followed about 20–25 days later by *Q. robur* and *T. cordata* (near DOY 115). All species generally reached 100 % leaf expansion by DOY 125–138, but latest until E (DOY 140). Leaf fall usually started between G (DOY 260) and H (290). The end of leaf fall was marked by point I (DOY 320). Although each species exhibited slight annual variation, the chosen cardinal points provide orientation throughout the year. The highest values for global radiation were reached at summer solstice (DOY 172), and the shortest day is at the winter solstice (DOY 355). Therefore, individual solar radiation thresholds were applied (500 W m^{-2} in Fig. 6 A, 650 W m^{-2} in Fig. 6 E, and 300 W m^{-2} in Fig. 6 F, G) for seasons with lower solar radiation (DOYs: 90, 260, 320, 355), to avoid unreasonable model extrapolation beyond the typical radiation ranges during the respective timepoints.

2.3. Generalized additive models

Temperature difference was modeled using hierarchical generalized additive models (GAMs). Hierarchical (mixed) models impose a structure where the relationship between predictor and response are organized in groups and where errors are correlated due to multiple observations with the same measurement devices (Hastie and Tibshirani, 1986; Wood, 2017). As described by Wood (2017), GAM is a modeling technique where the impact of the predictive variables is captured through smooth functions (Eq. 1).

$$g(E(Y)) = \alpha + \sum_{i=1}^{p} \widehat{f}_i(X_i) + \varepsilon \tag{1}$$

where Y is the dependent variable, E(Y) denotes the expected value and g(Y) denotes the link function that links the expected value to the predictor variables $X_i - X_p$. $f_i - f_p$ denote smooth, non-parametric functions, i.e. the shape of the parametric functions is fully determined by the data and ε denotes the residual error. Each smooth f_i or regression spline is represented by a sum of K simpler basis functions $(b_{j,k})$, multiplied by the corresponding coefficients $\beta_{j,k}$ which need to be estimated (Eq. 2).

$$f_j(x_j) = \sum_{k=1}^{k} (\beta_{j,k} \bullet b_{j,k}(x_k)) \tag{2}$$

The coefficients were estimated using penalized maximum likelihood (Eq. 3) using the fast restricted maximum likelihood algorithm (fREML; Wood 2011).

$$lr(\beta, \lambda) = \int f(y|\beta) f(\beta) d(\beta) + \lambda \int f''(t)^2 \tag{3}$$

The penalty in model estimation reduces some basis coefficients to zero, which reduces the degrees of freedom to effective degrees of freedom (EDF), with more EDF implying more complex splines (Wood, 2011). In addition, an extra penalty was added (double shrinkage), that if the smoothing parameter is large enough the coefficients will shrink to zero (Marra and Wood, 2011), which is useful to assess whether a predictor is adding anything to the model and can be used as variable selection technique and to avoid concurvity, the generalization of collinearity in a GAM setting. In the case of concurvity, the smooth term can be approximated by some combination of others and will result in unstable estimates. Further, the contribution of individual variables to the model were assessed using the "average shared variance method", for details see Lai et al. (2024).

The GAM models and the average shared variance were estimated with the *mgcv*-package (Wood, 2003, 2017; Wood et al., 2015, 2016) and the *gam.hp* package (Lai et al., 2024) in R (R Core Team, 2024). We fitted a temporal and a causal model to the data. In the temporal model, the temperature offset was modeled dependent on DOY, TOD for each of the seven species compositions and replications (28 pure and mixed plots in total). We included the interaction of DOY, TOD and species composition allowing daily patterns to vary by species and season, as well as a random effect for the sensor ID and year (Eq. 4). To capture seasonal and diurnal patterns, we used cubic regression splines placing knots for each month (k = 12) and each hour of the day (k = 24 and k = 12 for the DOY x TOD interaction).

$$\begin{aligned} T_{Off} &= f(speciescomp, DOY, bs = c(\text{“}fs\text{”}, \text{”}cc\text{”}) + f(speciescomp, TOD, bs \\ &= c(\text{“}fs\text{”}, \text{”}cc\text{”})) + f(species\ comp, TOD, DOY, bs \\ &= c(\text{“}fs\text{”}, \text{”}cc\text{”}, \text{”}cc\text{”}\ \ )) + f(SensorID, year, bs = \text{”}re\text{”}) \end{aligned} \tag{4}$$

Conversely, the causal model incorporated the most influential physical factors which were solar radiation, wind and relative air humidity (see Introduction). These climatic variables were selected based on the literature review. Models with these climate variables as main effects or main effects and interaction, were not able to capture diurnal and seasonal patterns adequately, as indicated by the model residuals. We therefore included diurnal patterns via a distributed lag model and included DOY in the solar radiation term. A distributed lag model (Wood, 2017) quantifies the influence of physical factors through the cumulative sum of smooth functions, each corresponding to different time lags of these factors. In our analysis, we selected a lag duration of 24 hours, aligning with the complete cycle of a day, to ensure all variables were assessed with a one-day delay. This model structure is reasonable, since the temperature offset response lags behind several of the physical variables found in the data set. For instance, maximum temperature would be achieved approximately 2 hours after the maximum radiation. With a potential up to 24 lags, the nighttime component of temperature offsets could also be modeled. Since neither air humidity nor wind speed have distinct seasonal patterns, for these variables no lagged component was fit. The most important stand variable is LAI (see Introduction), which was included in the model. To allow in addition for species specific stomatal response, the relative humidity term was smoothed species specific. Also, in this model a random effect for the sensor ID and year was included. Cubic regression splines were chosen for the lagged component and thin plate regression splines for all other model terms. The model is written in Eq. 5.

$$\begin{aligned} T_{Off} &= f(DOY, Rad_{solar}, lag, bs \\ &= \text{”}cr\text{”}\ \ ) + f(wind, bs = \text{″}tp\text{″}) + f(rel\ air\ humidity, species\ comp, bs \\ &= \text{”}fs\text{”}) + f(leaf\ area\ index, bs = \text{″}tp\text{″}) + f(SensorID, year, bs = re) \end{aligned} \tag{5}$$

Model residuals were homoscedastic, but heavy tailed and autocorrelated. Consequently, we chose the *scaled t*-distribution appropriate for heavy tailed data and fit an autoregressive AR1 model to the residuals. Autocorrelation was nested within year and sensor ID and the autocorrelation coefficient, ρ, was set to 0.9. This adaptation yielded the wanted distribution of the model residuals. Concurrent models were selected based on Akaike's information criterion (AIC) (Akaike, 1973) and on biological plausibility, for both the temporal and the causal model. R^2 and RMSE metrics were calculated for both models.

3. Results

3.1. Descriptive Statistics

Offsets between the forest temperature and open-field temperature varied between −12.5 °C and + 6.8 °C during the two observation years. On average the air under the forest canopy was −0.47 °C colder. Temperature offsets were positive at night and negative during the day, with the minimum and maximum varying by season and species composition (Table 2). Pairwise comparisons of the mean forest temperature and mean temperature offset revealed no significant differences ($p < 0.05$), except for the mean forest temperature between Qr and ApTc in spring.

B-Tree is still a young plantation forest in the pole stage and the average LAI is increasing from 2020 to 2022 (Fig. 2). Over all three years, the mixtures ApTc, QrCb and All are among the plots with the highest LAIs. Among the monocultures, *A. platanoides* holds similar high LAI values as the mixtures, except in 2020, where *Q. robur* was the monoculture with the highest LAI values. *A. platanoides* dominated the LAI of the mixtures, while *Q. robur* and *C. betulus* showed a more balanced share of LAI in mixtures. The LAI of *T. cordata* in mixtures was consistently low.

At the start of our campaign in 2020, *T. cordata* began leaf abscission around DOY 259, whereas *Q. robur* did not start until DOY 294, and *C. betulus* still maintained most of its foliage into late September. By DOY 320, *T. cordata* and *A. platanoides* had lost all leaves, while *Q. robur* and *C. betulus* retained about 10 % over the winter months. In 2021, A. *platanoides* and *C. betulus* reached bud break by DOY 91, while *Q. robur* and *T. cordata* started closer to DOY 115. That year, *T. cordata* initiated leaf shedding by DOY 244, whereas *C. betulus* started to shed its leaves by DOY 270, followed by *A. platanoides* by DOY 280, and *Q. robur* by DOY 300. Qr and Cb kept their foliage substantially longer (DOY 305–314). In 2022, *A. platanoides* and *C. betulus* began flushing around DOY 97, whereas *Q. robur* and *T. cordata* remained dormant until around DOY 119. By then, *A. platanoides* was already ~75% leafed out, and by DOY 138 all four-species had fully expanded crowns. Despite these minor shifts in timing, no substantial phenological differences were observed between mixtures and monocultures, as each species followed its general pattern regardless of stand composition Fig. 3.

3.2. Seasonal and diurnal temperature offsets

The temporal model explained 45.3 % of the deviance and 65.9 % (R^2) of the temperature variation, with a root mean square error (RMSE) of 1.13 °C. The model predicted maximum cooling effects of air temperature through forests of –6.00 °C and for warming effects + 2.40 °C.

Temperature offsets between the forest sub-canopy measurements and the open-field were positive in winter and negative in summer indicating a warming and cooling effect, respectively (Fig. 3, Supplementary Fig. A.2). For *A. platanoides*, the cooling effect started towards the end of bud break (Fig. 3, point D) and was c. −0.4 °C when leaf unfolding was completed (Fig. 3, point E) around mid-May. The maximum cooling effect in *A. platanoides* monocultures was observed at summer solstice (Fig. 3, point F) with an average cooling effect of c. −1.25 °C and cooling ceases when leaf fall is completed. The other monocultures and species mixtures showed similar seasonal patterns, modulated by phenology (Supplementary Fig. A.2) and species identity and is described further below.

Diurnal temperature cycles varied by season, exemplified for four characteristic time points throughout the year (Fig. 4). Temperature offsets were most pronounced around the summer solstice (Fig. 4 B) and least pronounced around the winter solstice (Fig. 4 D). End of bud break (Fig. 4 A) and the phenological start of fall (Fig. 4 C) showed tree species specific or intermediate temperature buffering, respectively.

Around bud break of the species *Q. robur* and *T. cordata* (30th April, DOY 120), *A. platanoides* and *C. betulus* stands had an early increase in cooling capacity (-1.7 °C) during the day and showed a higher warming effect during nighttime (+1.2 °C) compared to *Q. robur* and *T. cordata* (0 °C to +0.9 °C; Fig. 4). This reflects species dependent offsets in leaf flushing at the site (Fig. 3; Supplementary Fig. A.2). *A. platanoides* and *C. betulus* were the first species to start with leaf flushing (DOY 90) and showed a rapid leaf development, while the two other species were still dormant. *Q. robur* and *T. cordata* had a later start in leaf development resulting in a warming effect during daytime (+0.4 °C) around bud break (Supplementary Fig. A.2). During summer solstice (21st June, DOY 172) the complete set of the four species showed the highest cooling capacity of the year (-4.2 °C to −5.2 °C), whereby *A. platanoides* and *C. betulus* showed a more pronounced cooling than *Q. robur* and *T. cordata* (Fig. 4). The highest warming effect during summer (up to +1.5 °C) occurred during nighttime. With the main phenological start of the leaf shedding (17th September, DOY 260), the general cooling capacity of the stands declined to a maximum air temperature cooling of −3.1 °C shortly before noon and a reduction of the nightly warming to + 1.3 °C. Of all tree species, *T. cordata* initiated leaf shedding (very early in 2021 by DOY 244), which resulted in reduced air temperature cooling (Fig. 4 C). For winter solstice (21st December, DOY 355), the set of four species show little differences between night and day with temperature offsets ranging from −0.2 °C to + 0.7 °C. The four investigated broadleaf species had a higher nighttime air warming effect compared to the open-field during the peak of the vegetation season. Throughout the winter and early spring, lower warming effects (between +0.3 °C and +1.2 °C) occurred during nighttime.

Temperature offsets in mixture are exemplified for the summer

Table 2
Mean meteorological seasonal forest temperature under the canopy and mean temperature offsets between the forest and the open-field measurements per species composition, negative values indicating a lower air temperature under the tree canopies. Species composition abbreviations: Ap (***A**cer **p**latanoides*), Tc (***T**ilia **c**ordata*), Qr (***Q**uercus **r**obur*), Cb (***C**arpinus **b**etulus*), ApTc (***A**cer **p**latanoides* + ***T**ilia **c**ordata*), QrCb (***Q**uercus **r**obur* + ***C**arpinus **b**etulus*), All (four-species mixture). Asterisks * mark significant differences of the mean forest temperature between species compositions. (one-way ANOVA with Tukey's HSD test, $p < 0.05$; mean ± SD, $n = 4$).

Species composition	Season	Forest temperature [°C] ± SD	Temperature offset [°C] ± SD	Season	Forest temperature [°C] ± SD	Temperature offset [°C] ± SD
Ap	Spring	11.0 ± 6.8	−0.3 ± 2.1	Summer	20.6 ± 4.9	−1.0 ± 2.8
Tc	Spring	11.3 ± 6.9	−0.1 ± 1.6	Summer	20.5 ± 5.0	−1.1 ± 2.6
Qr	Spring	11.4 * ± 6.4	−0.1 ± 1.5	Summer	20.5 ± 5.0	−1.2 ± 2.5
Cb	Spring	10.9 ± 6.4	−0.4 ± 2.0	Summer	20.4 ± 4.8	−1.3 ± 2.7
ApTc	Spring	10.6 * ± 6.7	−0.7 ± 1.8	Summer	20.2 ± 4.9	−1.4 ± 2.6
QrCb	Spring	11.0 ± 6.9	−0.3 ± 1.7	Summer	20.5 ± 5.0	−1.1 ± 2.5
All	Spring	11.1 ± 6.9	−0.1 ± 1.8	Summer	20.7 ± 4.9	−0.9 ± 2.6
Ap	Autumn	11.1 ± 6.3	−0.3 ± 1.8	Winter	2.6 ± 4.3	−0.1 ± 0.7
Tc	Autumn	10.8 ± 6.4	−0.3 ± 1.7	Winter	2.6 ± 4.1	0.1 ± 0.6
Qr	Autumn	10.8 ± 6.2	−0.3 ± 1.8	Winter	2.5 ± 4.0	0.1 ± 0.7
Cb	Autumn	10.7 ± 6.2	−0.4 ± 1.8	Winter	2.4 ± 4.0	−0.1 ± 0.7
ApTc	Autumn	10.8 ± 6.3	−0.4 ± 1.8	Winter	2.5 ± 4.2	−0.1 ± 0.7
QrCb	Autumn	11.1 ± 6.2	−0.2 ± 1.8	Winter	2.8 ± 4.1	0.1 ± 0.7
All	Autumn	11.2 ± 6.2	−0.2 ± 1.8	Winter	2.8 ± 4.2	0.1 ± 0.6

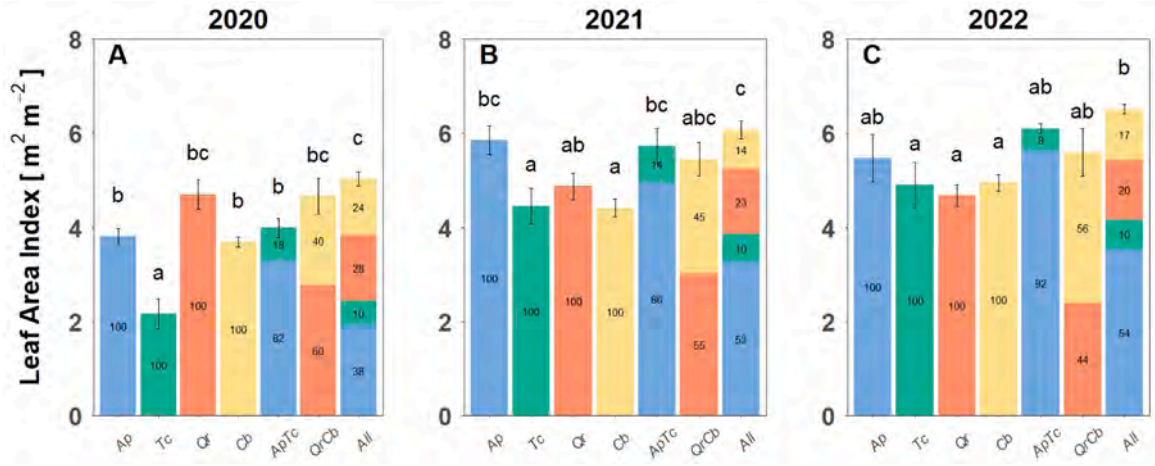

Fig. 2. Absolute leaf area index (LAI) at the B-Tree experimental site (Austria) in 2020 (**A**), 2021 (**B**) and 2022 (**C**). Numbers in the bars represent the proportional share of the tree species LAI compared to the absolute LAI in percent. Y-axis shows the absolute LAI in m^2 m^{-2}, and the x-axis shows the different plot compositions for the four monocultures Ap (***Acer platanoides***), Tc (***Tilia cordata***), Qr (***Quercus robur***), Cb (***Carpinus betulus***) and the three different tree species mixtures ApTc (***Acer platanoides*** + ***Tilia cordata***), QrCb (***Quercus robur*** + ***Carpinus betulus***), All (four-species mixture). Letters mark significant differences of the mean LAI between species compositions. (one-way ANOVA with Tukey's HSD test, $p < 0.05$; mean ± SE, n = 4).

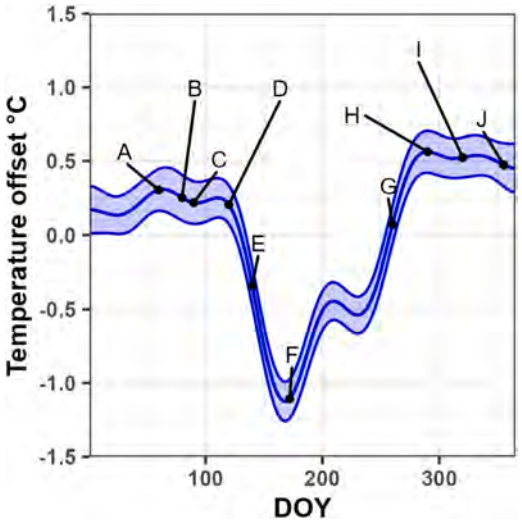

Fig. 3. Seasonal pattern of temperature offsets at time of day (TOD 12) for *A. platanoides* (blue line) with a 5% confidence interval band (transparent blue). The letters mark important time points throughout the season (see Supplementary Table **A.1**): A (DOY 60), B (DOY 80), C (DOY 90, bud break *A. platanoides* + *C. betulus*), D (DOY 120 end of bud break *Q. robur* + *T. cordata*), E (DOY 140 leaf unfolding finished), F (DOY 172, summer solstice), G (DOY 260, phenological start of leaf fall), H (DOY 290, leaf fall completed), I (DOY 320), J (DOY 355, winter solstice). Y-axis: Temperature offsets in °C between forest plots and open-field measurements in the year 2021, X-axis: Day of the year DOY.

solstice (21st of June, DOY 172), which showed the most pronounced cooling effects in monocultures (Fig. 5, Fig. 4 B). Around noon, all three mixtures / species compositions (ApTc, QrCb and All; Fig. 5) showed an intermediate effect on temperature offsets, depending on the performance of their respective monocultures (Fig. 5). Interestingly, during nighttime, the two-species mixtures ApTc and QrCb (Fig. 5 A, B) caused a distinctly reduced warming effect (Δ 0.3 °C and Δ 0.6 °C, respectively), than the respective monocultures. Similar, the four-species mixture (All) showed a temperature offset effect at noon in between those of the four monocultures, reaching a similar maximum cooling effect (-4.7 °C), however, the reduced warming effect compared to the monoculture during the night (with +0.4 °C) was less distinct compared to the two-species plots.

3.3. *Effects of solar radiation, wind, relative humidity, LAI and species composition on temperature variation*

Similar to the temporal model, the causal model explained 44.9 % of the deviance and 65.9 % (R^2) of the temperature variation, with a root mean square error (RMSE) of 1.13 °C. It estimated a slightly lower maximum cooling effect of −5.0 °C and a warming effect of + 1.48 °C than the temporal model.

3.4. *Solar radiation*

The 24-hour lagged solar radiation predictor is a proxy for radiation emissions during the day and night for the selected DOYs 90, 120, 140, 172, 260, 320 and 355 for an example species (Ap) (Fig. 6). The temperature buffering effect in early spring (Fig. 6 A, DOY 90) was characterized by a very flat lag0 curve, indicating an immediate forest warming effect between 0 and 300 W m^{-2} radiation and no cooling for higher radiation in spring. Lag1 – lag5 equally showed a slightly increasing cooling effect with rising radiation. Subsequent lags showed little to no response over the whole radiation range, with their maximum effect at −2 °C. With DOY 120 (Fig. 6 B), bud break was phenologically initiated. The leaf development differed between tree species (Supplementary Table A.1) and bud break started, depending on annual environmental factors, between DOY 90 and DOY 120. In Fig. 6 B, a slight warming effect for very low radiation values (60 W m^{-2}) could be still seen, which represented most likely dusk and dawn, followed by an increase in cooling capacity with higher radiation up to −1 °C. This effect could be explained with early leaf development stages of the forest canopy.

At DOY 140 (Fig. 6 C) full leaf expansion was reached, which strongly enhanced the forest cooling capacity. Here, the same radiative force caused a more pronounced forest cooling effect, resulting in a steeper curve for the first 5 lags. At 750 W m^{-2}, the air temperature was reduced by over 2.5 °C. Higher lags were now starting to show a slight positive trend with increasing solar radiation, indicating a shift in the pattern. With a continuation of the vegetation season and higher average temperatures during day and night in summer, forest cooling effects climaxed around summer solstice (DOY 172, Fig. 6 D). Forest cooling effects were positively correlated with solar radiation, almost reaching −4 °C of air temperature reduction with lag0. Although

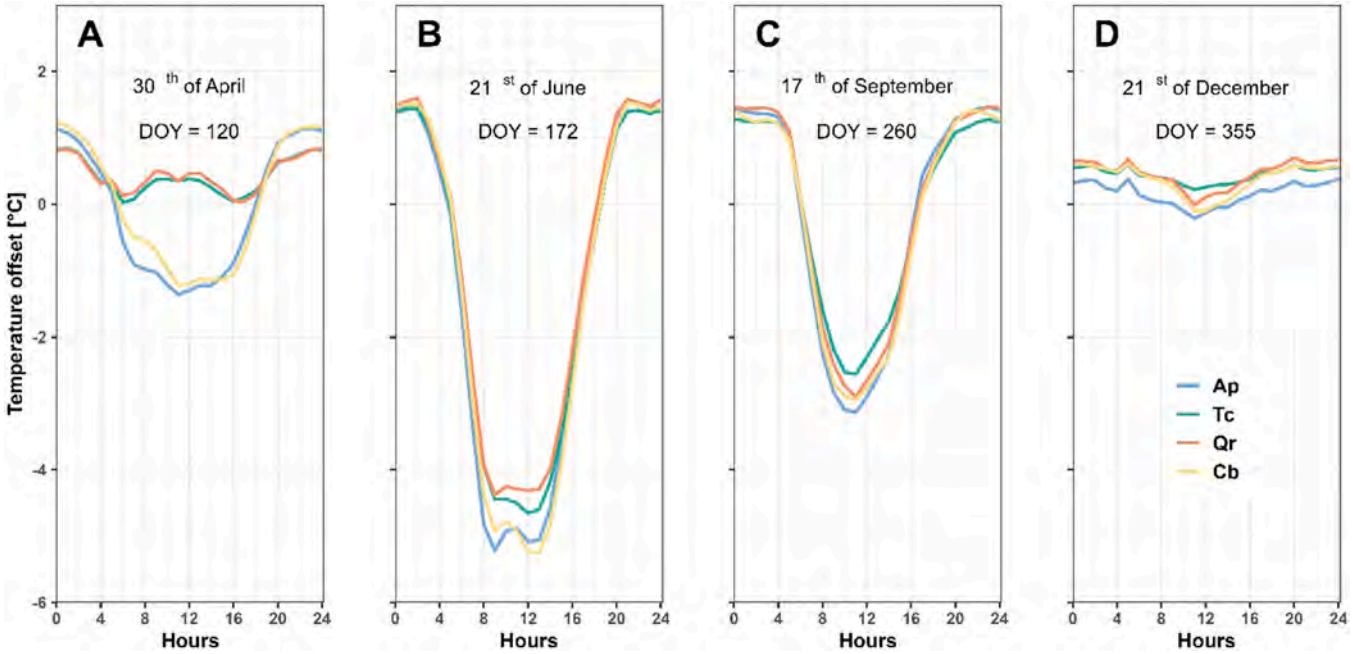

Fig. 4. Offsets in temperature between forest monoculture plots (***A**cer **p**latanoides* (Ap, blue), ***T**ilia **c**ordata* (Tc, green), ***Q**uercus **r**obur* (Qr, orange), ***C**arpinus **b**etulus* (Cb, yellow) and the open-field measurements in B-Tree, Austria. Subpanels show different temperature buffering effects of four different annual seasons **A:** DOY 120 (end of bud break), **B:** DOY 172 (summer solstice), **C:** DOY 260 (phenological start of leaf fall), **D:** DOY 355 (winter solstice). Y-axis: Temperature offsets in °C between forest plots and open-field measurements in the year 2021. X-axis: time of the day in hours.

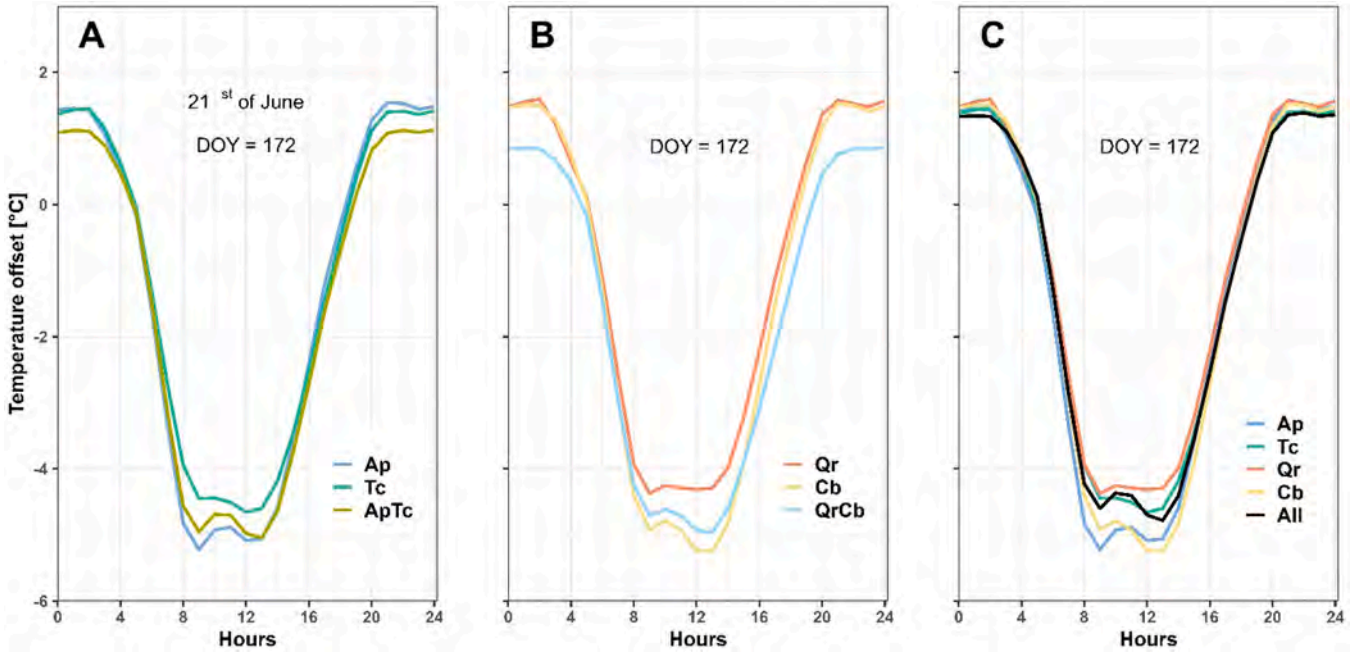

Fig. 5. Offsets in temperatures in mixed plots (ApTc, QrCb, All) compared to the respective monocultures at summer solstice (DOY 172); offsets calculated compared to open-field measurements in B-Tree, Austria. Subpanels (**A-C**) show temperatures in ApTc (dark green, A), QrCb (light blue, B), and All (black, C) stands. ApTc (***A**cer **p**latanoides* + ***T**ilia **c**ordata*), QrCb (***Q**uercus **r**obur* + ***C**arpinus **b**etulus*), All (four-species mixture) and their monocultures (Ap (blue), Tc (green), Qr (orange), Cb (yellow)). Y-axis: Temperature offsets in °C between forest plots and open-field measurements in the year 2021. X-axis: time of the day in hours.

showing significant cooling effects, prominent cooling effects decreased with increasing lag numbers (see lag 3–5 in Fig. 6 D). Unsurprisingly, the forest cooling capacity effects were most pronounced around summer solstice, 21st of June. The influence of radiation decreased with increasing lags. In late summer (DOY 260, Fig. 6 E), average day and night temperatures were still high, and the patterns are analogous to summer solstice results. However, the maximum cooling effect already started to decrease (maximum cooling about –3 °C at 600 W m^{-2}). At DOY 260, the pattern of the lags > 6 was reversed, which indicated increased radiation emissions during the night. With the start of fall and leaf shedding (DOY 320, Fig. 6 F) and winter solstice (DOY 355, Fig. 6 G), the curves flattened, and the cooling effect of the forest vanished and even went back to a slight warming effect around winter solstice with + 0.2 °C for 100 W m^{-2}.

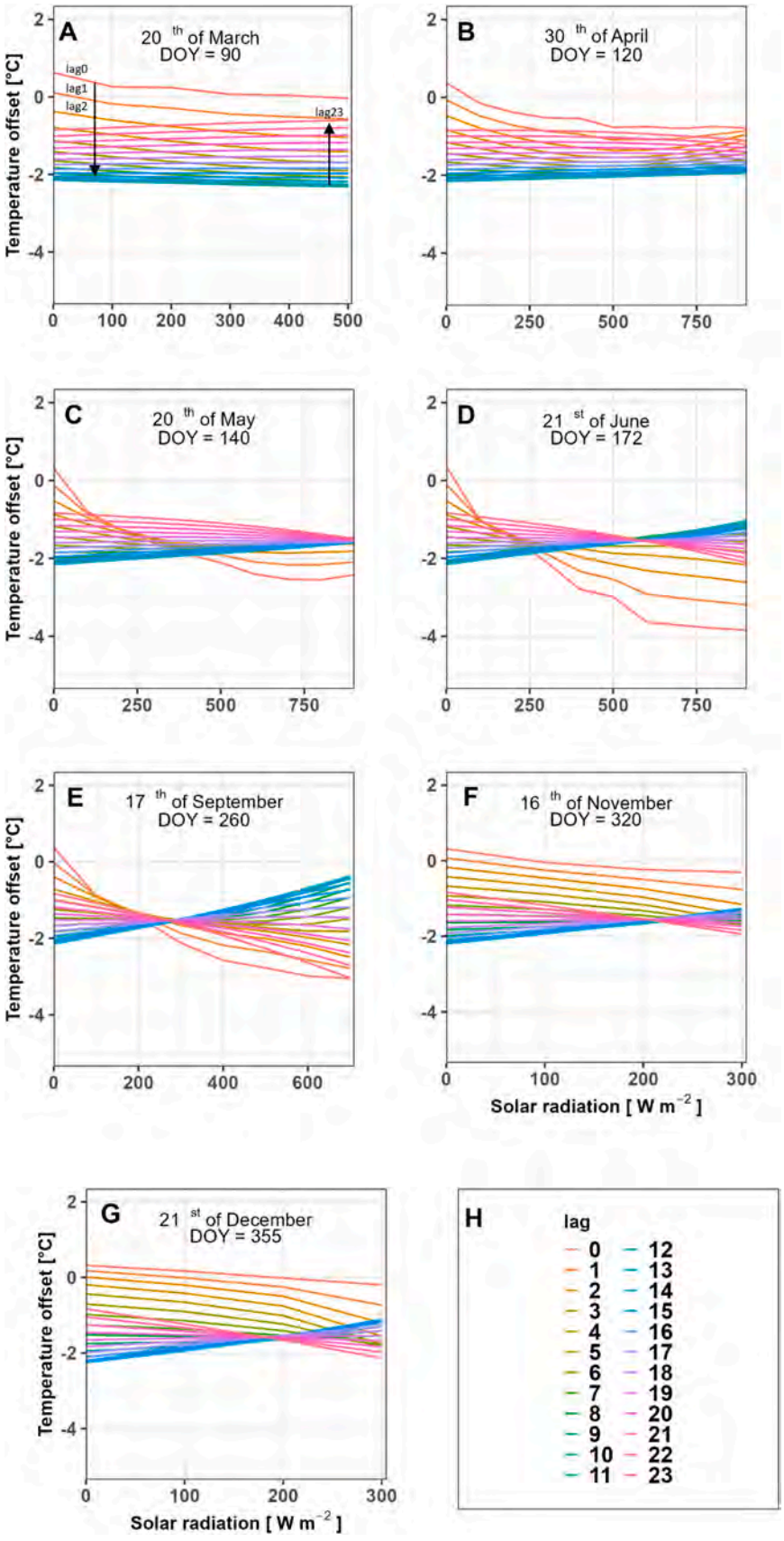

(caption on next page)

Fig. 6. Conditional plots of the causal model for a sequence of phenological dates (DOY 90, 120, 140, 172, 260, 320, 355) in the year 2021, listed in Supplementary Table **A.1**. Shown are the effects of solar radiation on the temperature buffering capacity of an example species (Ap2) in B-Tree, Austria. In the panels **A-G** the temperature buffering effect of the forest with 24 lags in one-hour timesteps from the start of spring **A:** DOY 90 until the winter solstice **G:** DOY 355 are shown. Panel **H** shows the 24 lags starting with lag0 in orange ending with lag23 in bright pink. Lag0 is the temperature estimation by the causal model for the given time, lag1 for the actual time + 1 hour and lag23 equals + 23 hours. Model parameters were fixed to 78 % relative humidity, LAI = 3.5 m^2 m^{-2}, wind = 2.7 m s^{-1}, representing the medians. Y-axis shows temperature offset between the forest and the open-field in °C and x-axis the solar radiation in W m^{-2}. X-axis scales vary due to different solar radiation regimes between seasons. The x-axis of low radiation timepoints are limited in a maximum solar radiation; **A**: DOY 90 to max. 500 W m^{-2}, **E:** DOY 260 to max. 700 W m^{-2}, and **F:** DOY 320 and **G:** DOY 355 to max. 300 W m^{-2}. The x-axis of high radiation timepoints **B:** DOY 120, **C:** DOY 140, **D:** DOY 172 is set to 875 W m^{-2}, corresponding to realistic values for these seasons.

The temporal lags of temperature offsets are exemplified for one of the forest plots (Ap2), which features *A. platanoides*, for multiple timepoints throughout the year (DOY 60 – 355; Fig. 7). DOY 60, 80 and 90 showed very little effect between 0 and 500 W m^{-2} with the stands still leafless. Around the bud break of the later species *Q. robur* and *T. cordata* (DOY 120), as opposed to the earliest species (DOY 90), a maximum cooling of ca. −0.8 °C was reached at 550 W m^{-2}. With rising solar radiation and ambient air temperature, the cooling capacity of forest stands increased. Subsequently this cooling effect was then modified and increased to ca. −2 °C by rapid leaf development of the tree species, only 20 days later (DOY 140) for the same radiation value. At summer solstice (21st of June, DOY 172), the curve reached its maximum cooling effect at 750 W m^{-2} of ca. −3 °C. With the beginning of autumn and decreasing ambient air temperatures and solar force, a reverse in the trend was detected and the cooling effect started to slightly decrease again. At the end of leaf fall, (DOY 290), the cooling effect and curve became even slightly flatter. Eventually, the lines for autumn and winter solstice (DOY 320, 355) approximated those of late winter / early string (DOY 60, 80, 90), although DOY 355 even showed a slight positive temperature effect for very low solar radiation (< 125 W m^{-2}).

3.5. Humidity, wind speed, and leaf area index

Tree species specific effects in temperature offsets in relation to the relative air humidity (macroclimatic) occurred (Fig. 8) and were displayed for summer solstice (21st June, DOY 172), anticipating the most pronounced temperature offsets (Fig. 7). We generally observed higher temperature offsets under drier macroclimatic conditions (i.e., lower relative humidity) across all species compositions, with subsequent species-specific responses emerging at distinct thresholds. In detail, *A. platanoides*, *Q. robur, T. cordata* and QrCb stands showed a turning point in temperature offset close to 45 % relative air humidity, where the biggest temperature offset was reached, with approx. −3.1 °C for *Q. robur* and *T. cordata*. The mixture ApTc and *A. platanoides* showed a similar response over the air humidity spectrum. The mixture QrCb had the least cooling capacity (-2.4 to −2.9 °C) throughout the humidity spectrum, but only a weak response to dropping relative humidity levels lower than 45 %. The mixture All, which includes all species, showed an intermediate response over all species and compositions, maintaining a stable cooling effect. *C. betulus* showed a high thermal cooling even during low relative air humidity values, surpassing all other species compositions at lower humidity levels than 75 %.

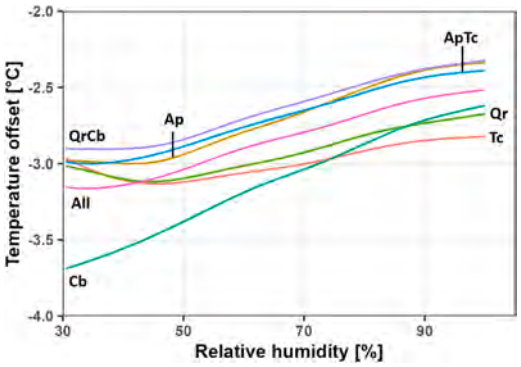

Fig. 8. On the y-axis the temperature offset between forest plots and the open-field is plotted in °C. The x-axis shows relative air humidity from 30 % to 100 %. The graph shows differences of tree composition responses to relative humidity for summer solstice (DOY 172) in the year 2021. Model parameters were fixed to 500 W m^{-2}, LAI = 3.5 m^2 m^{-2}, wind = 2.7 m s^{-1}, representing the medians. Shown are the three mixtures ApTc (***A**cer **p**latanoides* + ***T**ilia **c**ordata*), QrCb (***Q**uercus **r**obur* + ***C**arpinus **b**etulus*), All (four-species mixture), and the monocultures of their constituent tree species Ap, Tc, Qr, Cb.

For wind speeds below 7.5 m s^{-1} we saw a cooling effect throughout the different plots in B-Tree (Fig. 9). With increasing wind speeds, the

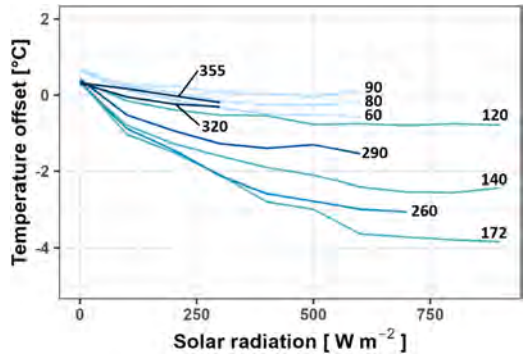

Fig. 7. Temperature offsets between one of the forest plots (Ap2) and the open-field in °C (y-axis) and the solar radiation in W m^{-2} (x-axis) across the year 2021 (DOY 60–355) in different colored lines for lag0 of the model. Model parameters were fixed to 78 % relative humidity, LAI = 3.5 m^2 m^{-2}, wind = 2.7 m s^{-1}, representing the medians. The lines are cut for non-realistic solar radiation values for the corresponding time of the year.

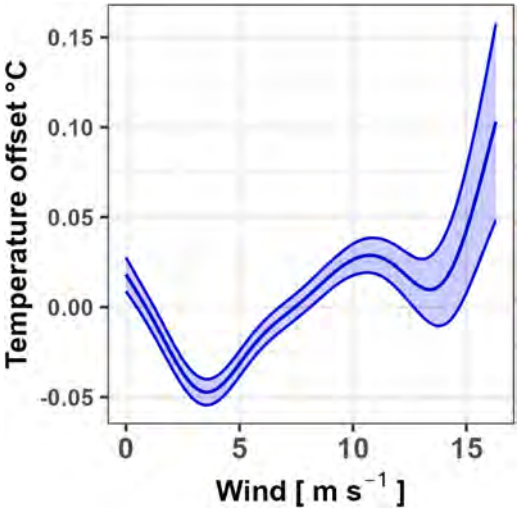

Fig. 9. On the y-axis the temperature offset between forest plots and the open-field is plotted in °C. On the x-axis wind in m s^{-1}. A 5 % lower and upper confidence interval was calculated for the temperature offset. We fixed the solar radiation to 500 W m^{-2}, the relative humidity and the LAI to their medians, 78 % and 3.5 m^2 m^{-2}, respectively.

cooling effect vanished, and a warming effect could be identified. A very pronounced increase was found for the highest observed wind speeds of c. 15 m s^{-1} (Fig. 9). Temperature difference almost linearly increased with increasing LAI (Fig. 10), but only within a small temperature magnitude (-0.3 °C to +0.3°C).

4. Discussion

We utilized high-resolution temporal data from a homogenous experimental forest to explore temperature disparities between the forest and the open-field. Our analysis included direct LAI measures, which is rarely done in similar research. The temporal and the causal model, fitted using generalized additive models, allowed for a detailed analysis of species-specific, diurnal and seasonal patterns of hourly temperature data and allowed to quantify the effects of mixture on microclimate. Contrary to our expectations, the causal model, incorporating solar radiation, wind speed, relative air humidity and LAI did not significantly outperform the temporal model in explaining the temperature variation offsets. Both models fit the data equally well, with a R^2 of 66 % and RMSE of 1.13°C. There were slight differences in the minimum and maximum predicted temperature offsets.

The temporal model predicted maximum cooling effects of air temperature through forests of –6.00 °C and for warming effects + 2.40 °C. Meanwhile, the causal model estimated a slightly lower maximum cooling effect of −5.0 °C and a warming effect of + 1.48 °C. The cooling effects are notably higher than the monthly temperature offsets reported in existing literature, such as Haesen et al. (2021) with cooling of −2.1 ± 1.6 °C in summer and warming of + 2.0 ± 0.7 °C in winter, or De Lombaerde et al. (2022), predicting global forest temperature offsets of −2.92 ± 1.57 °C for cooling and + 0.96 ± 1.27 °C for warming. De Frenne et al. (2019) reports a global mean cooling effect of forests of −4.1 ± 0.5 °C and a warming effect of + 1.1 ± 0.2 °C compared to open habitats, while Zhang et al. (2022) reported −1.8 ± 2.6 °C (mean ± SD) and + 0.6 ± 2.1 °C for daily maxima in summer and daily minima in winter. Our findings are of similar magnitude with Upreti et al. (2017), who also account for diurnal temperature variation. Generalized Additive Models (GAMs) can capture nuanced diurnal shifts well throughout the year and effectively model complex, nonlinear relationships without the need for predefined forms, although their optimal performance hinges on the careful selection of smoothness and requires large datasets and significant computational power (Wood, 2017). The multi-annual

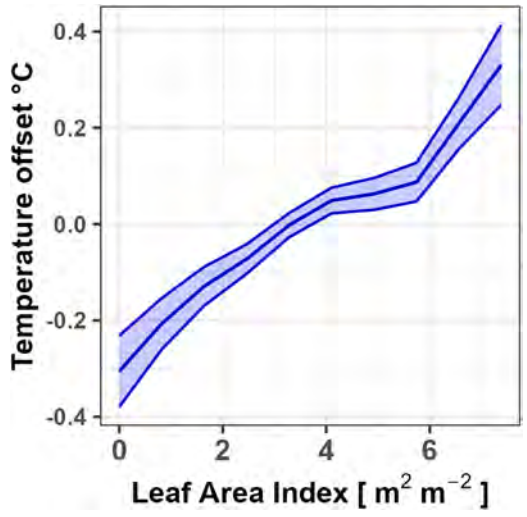

Fig. 10. On the y-axis the temperature offset between forest plots and the open-field is plotted in °C. Leaf area index in m^2 m^{-2} (LAI) on the x-axis. A 5 % lower and upper confidence interval was calculated for the temperature offset. We fixed the solar radiation to 500 W m^{-2}, relative humidity and the wind to their median, 78 % and 2.7 m s^{-1}, respectively.

dataset with 3-hourly precision provides the quantity of data for these models. Acknowledging the limitations of the temperature micro-loggers, we note that deploying these loggers under forest canopies during vegetation season helps mitigate radiation influence naturally. Nevertheless, we used functioning radiation shields for all sensors, including those in open-fields and during the leaf-off season, to further reduce sensor bias (Lundquist and Huggett, 2008; Maclean et al., 2021a; Terando et al., 2017; van de Pol et al., 2016). Despite potential concerns over the sensor accuracy, such devices, validated by studies (Koenig et al., 2015, 2017; Quadri et al., 2021), offer reliable data for ecological research.

Our study distinguishes itself by considering hourly temperature cycles, leading to higher offset values. Furthermore, our analysis focused on pure deciduous broadleaf stands, diverging from other studies' inclusion of coniferous trees, which resulted in only marginal warming effects in winter. It is crucial to note whether offsets are based on daily averages or daily maximum temperature buffering, which is significant for plant and human health. The specifics of each model are elaborated in the subsequent sections.

4.1. Temporal model

The temporal model provides a robust framework for capturing the general temperature dynamics within forest ecosystems, adeptly reflecting the mean diurnal, weekly, monthly, seasonal, and yearly temperature responses of various tree species. Fig. 3 illustrates the consistent seasonal temperature patterns, with significant deviations corresponding to key phenological events, suggesting that the model is well-suited for capturing the overall trends of canopy-driven microclimate regulation. However, its ability to predict temperature extremes and peaks is constrained, largely due to its exclusion of weather conditions. While it aptly reflects an average temperature trajectory, as one might observe on a standard July day, it fails to encapsulate the acute variations associated with sudden climatic perturbations. Nevertheless, the high temporal resolution of the model allows to model even species specific phenological responses to temperature buffering (Fig. 4 A).

The diurnal temperature fluctuations play a critical role in plant physiology, influencing key processes such as photosynthesis, respiration, heat stress, and winter hardening (De Frenne et al., 2021; Gallou et al., 2023), which are more responsive to temperature extremes than to monthly means. Our temporal model is capable of capturing these diurnal temperature patterns, filling a gap left by many models that typically focus on seasonal rather than daily variations. Although diurnal effects are recognized for their significance, there remains a scarcity of models that uniformly depict these fluctuations across different seasons. In a similar study, Schnabel et al. (2024) documented a notable temperature buffering effect in young forest plantations, with maximum cooling observed during midday (-2.5 ± 0.2 °C) and warming effects peaking at midnight (+0.4 ± 0.04 °C). However, their study did not account for the interplay between seasonal and diurnal cycles. Our research aligns with their findings on the overall impact of forest temperature buffering but also elucidates the varying diurnal amplitudes across different seasons. In the spring, temperature buffering capacities are distinctly influenced by interspecies variations in phenological events such as leaf flushing. The phenological sequence—*Carpinus betulus*, *Acer platanoides*, *Quercus robur*, and *Tilia cordata*—remains consistent annually, with the time span for leaf emergence varying between 13 and 17 days, and even up to 20–26 days across different years (Wesołowski and Rowiński, 2006). Autumn litter fall follows the reverse order of spring flushing, with *C. betulus* experiencing the longest leaf duration of 191 days, followed by *Q. robur* with 186 days and *A. platanoides* with 180 days, corroborating the findings for *C. betulus* and *Q. robur* by Asshoff et al. (2006). *T. cordata* had the shortest leaf duration of 134 days, which is consistent with previous observations (De Jaegere et al., 2016). Research on leaf fall triggers is limited, yet these species-specific leaf durations significantly influence annual cooling

capacity.

Our results reveal distinct species-specific cooling capabilities linked to differences in LAI, with *A. platanoides* and *C. betulus* outperforming *T. cordata* and *Q. robur*, particularly noticeable at summer solstice (Fig. 5). The higher LAI and prolonged leaf duration of *A. platanoides* and *C. betulus* suggest enhanced temperature buffering effect throughout the year. *T. cordata* and *A. platanoides* utilize their thinner leaves and simpler shapes for effective transpirative cooling, emphasizing the role of leaf morphology in microclimate regulations (Gebauer et al., 2012; Rahman et al., 2020). Conversely, the sparse canopy of *Q. robur* results in the smallest temperature buffering effect among the studied broad-leaved species, despite its ability to maintain high transpiration rates during water scarcity (Leuzinger and Körner, 2007). Tree species mixtures showed stronger cooling effects than would be expected from the constituent species in monoculture, the cooling effect of the mixture was almost as large as that of the better cooling species, however never larger. Our findings corroborate the critical influence of canopy density and structure on temperature buffering, significantly impacting temperature buffering, as they modulate solar radiation interception and transpiration (Zhang et al., 2022; Schnabel et al., 2024). This is supported by the work of Leuzinger and Körner (2007), who identified canopy density as a pivotal factor in temperature regulation within mixed-species forests. Our studied forest stands had a considerable buffering capacity despite their early developmental stage, supporting previous findings (Gillerot et al., 2022; Zhang et al., 2022; Schnabel et al., 2024). Mature forests typically demonstrate stronger cooling effects and diminished diurnal temperature variations, suggesting a trend towards greater microclimatic stability in our study site over time (Gillerot et al., 2022; Lindenmayer et al., 2022).

The insights gained from our temporal model point to the significant role of species composition, phenology, and canopy structure in forest microclimate regulation. The model emphasizes the need for incorporating species-specific physiological traits and interactions in predictive models to enhance our understanding of ecosystem functioning.

4.2. Causal model

Temperature offsets were modeled using causal predictors. A significant challenge we faced was the concurvity or collinearity among the climatic covariates and the subsequent variable selection. To address this, we guided our variable selection based on those commonly used in the existing literature. Global radiation, relative air humidity, wind speed, air temperature and precipitation were used as a set of macroclimatic variables affecting the microclimate (Chen et al., 1999; Maclean et al., 2021b) on hourly basis.

During the day, tree canopies provide shade and evapotranspirate, lowering surface temperature by absorbing shortwave radiation (Hutchison and Matt, 1977; Zellweger et al., 2019). Conversely, at night, particularly where tree cover is high, outgoing longwave radiation might be trapped leading to warmer temperatures. This effect is counterbalanced by daytime shading and is pronounced in areas with high tree cover, where cooler daytime soil temperatures extend the cooling effect into the night (Meili et al., 2021). The causal model demonstrated a limitation in predicting nighttime temperatures due to the absence of a variable indicating long wave radiation emission (Von Arx et al., 2012). The introduction of a 24-hour lagged solar radiation predictor (Fig. 6) partly compensated for this lack of direct nighttime outgoing radiation measures, by inferring proportionality between the daytime incoming radiation measured. This improved the model's performance at night, capturing the essential cooling cycles. Measured incoming solar radiation was an excellent predictor explaining almost the entire variation of temperature offsets.

The model indicated that wind speed inversely affects temperature offsetting (Fig. 9), likely due to the open agricultural fields surrounding the study forest, leading to higher temperatures within the forest with increased lateral transfer of heat (Geiger et al., 2009). This is expected to reverse at night, but our study did not measure detailed wind profiles or canopy surface roughness, which are typically considered in mechanistic models (Meili et al., 2021). Although all of our sensors were placed in the center of stands, wind can modulate possible edge effects, which potentially penetrate and alter the microclimate of our relatively small experimental forest (Baker et al., 2016). However, studies with similar plot design do not discuss edge effects (Gillerot et al., 2022; Zhang et al., 2022; Schnabel et al., 2024), we acknowledge that the microclimate is impacted by forest edges with varying distances (Davies-Colley et al., 2000; Ewers and Banks-Leite, 2013).

The potential forest temperature buffering capacity is higher under drier conditions (Fig. 8), which is in agreement with Zhang et al. (2022) and Von Arx et al. (2012). However, below 30 % relative air humidity, model confidence intervals are large due to scarcity in data. Low values of relative air humidity additionally influence several other possible factors, such as soil water deficiency, closure of stomata, high temperatures with high evaporation demands of dry air. *C. betulus* showed a high thermal cooling even during low relative air humidity values, which might indicate very late closure of the stomata.

The LAI is the primary driver for cooling, indicating the significance of foliage traits and density in solar radiation transmission through the canopy (Von Arx et al., 2013; Hardwick et al., 2015; Rahman et al., 2020). Species diversity enhances canopy density and structural complexity, often leading to higher LAI in mixed stands compared to monospecific stands, a phenomenon known as overyielding (Pretzsch, 2014, 2019; Jucker et al., 2015; Pretzsch et al., 2016). These mixtures exploit different ecological niches, enhancing microclimate regulation through varied canopy architecture and drought resistance (Ehbrecht et al., 2017; del Río et al., 2021; Urgoiti et al., 2022; Zhang et al., 2022). This positively enhanced cooling effect can be explained by niche complementary, in particular an improved filtering of incoming radiation by the combination of light demanding and shade tolerant tree species as also observed by Zhang et al. (2022). Typically, the investigated tree species form two-layered stands, resulting in a better vertical distribution of foliage also beneficial for cooling (Ehbrecht et al., 2019). Particularly notable mixture effects are seen in combinations like light-demanding *Q. robur* with shade-tolerant *C. betulus*, and *A. platanoides with T. cordata*. However, in the latter pairing, *A. platanoides* begins to dominate over *T. cordata* (Fig. 2). The elevated LAI in these mixtures leads to enhanced cooling effects compared to what would be expected from the individual species (Fig. 5). However, an anomaly occurred in 2020 when *Q. robur* led in LAI, suggesting variability in leaf area linked to annual climatic fluctuations, a pattern also reflected in tree growth studies (Strieder and Vospernik, 2021; Vospernik et al., 2023). Intriguingly, the four-species mixture exhibited the highest LAI but only an intermediate thermal buffering capacity. This suggests that any overyielding effects in these mixtures are less significant than in two-species combinations, possibly due to balancing positive niche complementarity against competition among species with similar traits (Werner et al., 2024). Nevertheless, the contribution of species mixtures to thermal buffering is nuanced and varies by specific species combinations and site conditions (Gillerot et al., 2022; Zhang et al., 2022; Schnabel et al., 2024). In addition to the species and mixture effects mostly attributable to differences in LAI, there was a small additional LAI effect, which reflects between plot and between year differences in LAI. Within the same species, a denser canopy seems to slightly decrease cooling effects (Fig. 10). Note, however, that all our plots exhibited full crown closure in all three years studied.

Precipitation was found to be a weak predictor of temperature offsets, likely due to the monthly temporal resolution of the data. It is also possible that the impact of precipitation is significantly delayed, meaning it could influence temperatures, particularly if there are considerable hot days following that could be mitigated through evapotranspiration (ET). Tree evapotranspiration emerged as a critical factor in air temperature regulation, more effectively cooling the air when tree cover is dense (Von Arx et al., 2013; Zellweger et al., 2019;

Haesen et al., 2023). Nonetheless, due to its proxy nature for various parameters and the resulting collinearity, evapotranspiration was omitted from the final causal model.

The applicability of our models is limited to lowland areas with specific radiation regimes. In higher elevations, differing radiation and temperature conditions necessitate tailored modeling approaches for accurate temperature buffering predictions by forests.

5. Conclusions

We investigated four understudied broadleaf species, namely small-leaved lime (*Tilia cordata* Mill.), Norway maple (*Acer platanoides* L.), common hornbeam (*Carpinus betulus* L.), and pedunculate oak (*Quercus robur* L.), and compared monocultures versus mixtures for their temperature buffering effect. Species identity and corresponding traits, such as LAI and phenology, strongly modify these effects, with air temperature buffering being most pronounced around summer solstice. The macroclimatic variables solar radiation, relative air humidity, wind speed and LAI played significant roles in modeling temperature offsets between open-field and forest. *A. platanoides* and *C. betulus* showed earlier air temperature cooling in spring and higher cooling capacities than *Q. robur* and *T. cordata* during summer. Although an overyielding effect in terms of LAI was already described in our experimental forests, we also found a similar enhancement of temperature buffering capacity for the two-species and four-species mixtures – a benefit for ecosystem services that remains underreported in many studies.

Responses of mixed species compositions on air temperature showed increased cooling effects compared to the constituent species with the least cooling capacity. The two-species mixtures provided temperature buffering capacities nearly matching their highest-performing monoculture, reflecting strong niche complementary but not surpassing the top single species. In contrast, the four-species mixture achieved highest LAI, yet showed only intermediate temperature buffering, suggesting competition among similar species traits reduced overall gains.

These results have direct practical implications for forest managers and urban planners, especially in regions facing increased temperature variability. For example, *A. platanoides* and *C. betulus* may be prioritized in areas where enhanced cooling is desired. Our findings support the use of diverse forest stands and species selection to enhance thermal stability, human thermal comfort, and forest resilience. Mixed-species plantings can be strategically used in urban forestry efforts to optimize climate adaptation benefits.

To get a better general understanding of the air temperature buffering effect of forests and its effects on human health, future research should examine a wider range of forest types, age classes, and tree species compositions (including conifers) across altitudinal gradients. This would help refine species selection and stand composition strategies to maximize ecosystem services under changing climate conditions.

Funding

This research was initiated through the 2018–2019 BiodivERsA joint call for research proposals, under the BiodivERsA3 ERA-Net COFUND program, and with the funding organizations DFG (Germany), ANR (France), FWO (Belgium), FWF (Austria) and NCN (Poland). The work was funded by the FWF project I 4372-B to DLG and by the Dr. Forest project I 4411 to DH. BR and DLG were funded by the EU Horizon project EXCELLENTIA [grant number 101087262] at Mendel University in Brno during the manuscript preparation phase. QWG was supported by the BiodivClim ERA-Net COFOUND program (MixForChange), and by the FWF [grant number I 50086-B].

CRediT authorship contribution statement

Vospernik Sonja: Writing – review & editing, Writing – original draft, Visualization, Software, Methodology, Formal analysis. **Guo Qiwen:** Writing – review & editing, Methodology. **Haluza Daniela:** Writing – review & editing, Funding acquisition. **Godbold Douglas L.:** Writing – review & editing, Supervision, Funding acquisition, Conceptualization. **Rewald Boris:** Writing – review & editing, Methodology. **Gillerot Loïc:** Writing – review & editing, Writing – original draft, Validation, Supervision. **Steinparzer Matthias:** Writing – review & editing, Writing – original draft, Validation, Software, Methodology, Investigation, Formal analysis, Data curation, Conceptualization.

Declaration of Generative AI and AI-assisted technologies in the writing process

During the preparation of this work the authors used OpenAI's large-scale language-generation model with GPT-4.0 to improve the spelling and grammar of drafted sentences or text passages. After using this tool, the authors reviewed and edited the content as needed and take full responsibility for the content of the publication.

Declaration of Competing Interest

The authors declare that they have no known competing financial interests or personal relationships that could have appeared to influence the work reported in this paper.

Acknowledgements

The authors thank Josef Gardermaier for the inspiring discussions on the usage of GAMs for modeling time series and the master students Paulina Vásquez Quintana and Matthias Steckert for helping to measure the leaf area index data for 2022. We would like to thank Hans Sandén for site preparation and maintenance 2012–2023, Matthias Fidesser for helping with site preparation, and Mike Bambrick, Thorsten Berger, Pétra Berger, Ortal Rewald, and Taru Sandén, and students for helping with tree planting. Ramona Werner and Ivo Offenthaler thankfully helped with the overview of the B-Tree experimental forest.

Appendix A. Supporting information

Supplementary data associated with this article can be found in the online version at doi:10.1016/j.foreco.2025.122582.

Data availability

Data will be made available on request.

References

Akaike, H., 1973. Information theory as an extension of the maximum likelihood principle. In: Petrov, B.N., Csaksi, F. (Eds.), Second International Symposium of Information Theory. Akademiai Kiado, Budapest, pp. 267–281.

Ammer, C., 2019. Diversity and forest productivity in a changing climate. N. Phytol. 221, 50–66. https://doi.org/10.1111/nph.15263.

Asshoff, R., Zotz, G., Körner, C., 2006. Growth and phenology of mature temperate forest trees in elevated CO2. Glob. Chang. Biol. 12, 848–861. https://doi.org/10.1111/j.1365-2486.2006.01133.x.

Aussenac, G., 2000. Interactions between forest stands and microclimate: Ecophysiological aspects and consequences for silviculture. Ann. For. Sci. 57, 287–301. https://doi.org/10.1051/forest:2000119.

Baker, T.P., Jordan, G.J., Baker, S.C., 2016. Microclimatic edge effects in a recently harvested forest: Do remnant forest patches create the same impact as large forest areas? For. Ecol. Manag. 365, 128–136. https://doi.org/10.1016/j.foreco.2016.01.022.

Bramer, I., Anderson, B.J., Bennie, J., Bladon, A.J., De Frenne, P., Hemming, D., Hill, R. A., Kearney, M.R., Körner, C., Korstjens, A.H., Lenoir, J., Maclean, I.M.D., Marsh, C. D., Morecroft, M.D., Ohlemüller, R., Slater, H.D., Suggitt, A.J., Zellweger, F., Gillingham, P.K., 2018. Advances in Monitoring and Modelling Climate at Ecologically Relevant Scales. Adv. Ecol. Res. 58, 101–161. https://doi.org/10.1016/bs.aecr.2017.12.005.

Chen, J., Saunders, S.C., Crow, T.R., Naiman, R.J., Brosofske, K.D., Mroz, G.D., Brookshire, B.L., Franklin, J.F., 1999. Microclimate in forest ecosystem and landscape ecology: Variations in local climate can be used to monitor and compare

the effects of different management regimes. Bioscience 49, 288–297. https://doi.org/10.2307/1313612.
R. Core Team, 2024. _R: A Language and Environment for Statistical Computing_. R Foundation for Statistical Computing, Vienna, Austria. ⟨https://www.r-project.org/⟩.
D'Odorico, P., He, Y., Collins, S., De Wekker, S.F.J., Engel, V., Fuentes, J.D., 2013. Vegetation-microclimate feedbacks in woodland-grassland ecotones. Glob. Ecol. Biogeogr. 22, 364–379. https://doi.org/10.1111/geb.12000.
Davies-Colley, R.J.T., Payne, G.W., van Elswijk, M., Elswijk, M., 2000. Microclimate gradients across a forest edge. New Zeal. Ecol. Soc. 24, 111–121.
De Frenne, P., Lenoir, J., Luoto, M., Scheffers, B.R., Zellweger, F., Aalto, J., Ashcroft, M. B., Christiansen, D.M., Decocq, G., De Pauw, K., Govaert, S., Greiser, C., Gril, E., Hampe, A., Jucker, T., Klinges, D.H., Koelemeijer, I.A., Lembrechts, J.J., Marrec, R., Meeussen, C., Ogée, J., Tyystjärvi, V., Vangansbeke, P., Hylander, K., 2021. Forest microclimates and climate change: Importance, drivers and future research agenda. Glob. Chang. Biol. 27, 2279–2297. https://doi.org/10.1111/gcb.15569.
De Frenne, P., Rodríguez-Sánchez, F., Coomes, D.A., Baeten, L., Verstraeten, G., Vellen, M., Bernhardt-Römermann, M., Brown, C.D., Brunet, J., Cornelis, J., Decocq, G.M., Dierschke, H., Eriksson, O., Gilliam, F.S., Hédl, R., Heinken, T., Hermy, M., Hommel, P., Jenkins, M.A., Kelly, D.L., Kirby, K.J., Mitchell, F.J.G., Naaf, T., Newman, M., Peterken, G., Petřík, P., Schultz, J., Sonnier, G., Van Calster, H., Waller, D.M., Walther, G.R., White, P.S., Woods, K.D., Wulf, M., Graae, B. J., Verheyen, K., 2013. Microclimate moderates plant responses to macroclimate warming. Proc. Natl. Acad. Sci. U. S. A. 110, 18561–18565. https://doi.org/10.1073/pnas.1311190110.
De Frenne, P., Zellweger, F., Rodríguez-Sánchez, F., Scheffers, B.R., Hylander, K., Luoto, M., Vellend, M., Verheyen, K., Lenoir, J., 2019. Global buffering of temperatures under forest canopies. Nat. Ecol. Evol. 3, 744–749. https://doi.org/10.1038/s41559-019-0842-1.
De Jaegere, T., Hein, S., Claessens, H., 2016. A review of the characteristics of small-leaved lime (Tilia cordata Mill.) and their implications for silviculture in a changing clima. Forests 7, 1–21. https://doi.org/10.3390/f7030056.
De Lombaerde, E., Vangansbeke, P., Lenoir, J., Van Meerbeek, K., Lembrechts, J., Rodríguez-Sánchez, F., Luoto, M., Scheffers, B., Haesen, S., Aalto, J., Christiansen, D. M., De Pauw, K., Depauw, L., Govaert, S., Greiser, C., Hampe, A., Hylander, K., Klinges, D., Koelemeijer, I., Meeussen, C., Ogée, J., Sanczuk, P., Vanneste, T., Zellweger, F., Baeten, L., De Frenne, P., 2022. Maintaining forest cover to enhance temperature buffering under future climate change. Sci. Total Environ. 810. https://doi.org/10.1016/j.scitotenv.2021.151338.
Ehbrecht, M., Schall, P., Ammer, C., Seidel, D., 2017. Quantifying stand structural complexity and its relationship with forest management, tree species diversity and microclimate. Agric. For. Meteorol. 242, 1–9. https://doi.org/10.1016/j.agrformet.2017.04.012.
Ehbrecht, M., Schall, P., Ammer, C., Fischer, M., Seidel, D., 2019. Effects of structural heterogeneity on the diurnal temperature range in temperate forest ecosystems. For. Ecol. Manag. 432, 860–867. https://doi.org/10.1016/j.foreco.2018.10.008.
Ewers, R.M., Banks-Leite, C., 2013. Fragmentation Impairs the Microclimate Buffering Effect of Tropical Forests. PLoS One 8. https://doi.org/10.1371/journal.pone.0058093.
Fox, J., Weisberg, S., 2019. _An R Companion to Applied Regression_, Third edition. Sage, Thousand Oaks CA. ⟨https://socialsciences.mcmaster.ca/jfox/Books/Companion/⟩.
Gallou, A., Jump, A.S., Lynn, J.S., Field, R., Irl, S.D.H., Steinbauer, M.J., Beierkuhnlein, C., Chen, J.C., Chou, C.H., Hemp, A., Kidane, Y., König, C., Kreft, H., Naqinezhad, A., Nowak, A., Nuppenau, J.N., Trigas, P., Price, J.P., Roland, C.A., Schweiger, A.H., Weigelt, P., Flantua, S.G.A., Grytnes, J.A., 2023. Diurnal temperature range as a key predictor of plants' elevation ranges globally. Nat. Commun. 14. https://doi.org/10.1038/s41467-023-43477-8.
Gebauer, T., Horna, V., Leuschner, C., 2012. Canopy transpiration of pure and mixed forest stands with variable abundance of European beech. J. Hydrol. 442–443, 2–14. https://doi.org/10.1016/j.jhydrol.2012.03.009.
Geiger, R., Aron, R.H., Todhunter, P., 2009. The climate near the ground, 5th ed. Vieweg +Teubner Verlag, Wiesbaden. https://doi.org/https://doi.org/10.1007/978-3-322-86582-3.
GeoSphere Austria [WWW Document], 2023. URL ⟨https://data.hub.geosphere.at/dataset/⟩ (accessed 6.1.23).
Gillerot, L., Landuyt, D., De Frenne, P., Muys, B., Verheyen, K., 2024a. Urban tree canopies drive human heat stress mitigation. Urban For. Urban Green. 92, 128192. https://doi.org/10.1016/j.ufug.2023.128192.
Gillerot, L., Landuyt, D., Oh, R., Chow, W., Haluza, D., Ponette, Q., Jactel, H., Bruelheide, H., Jaroszewicz, B., Scherer-Lorenzen, M., De Frenne, P., Muys, B., Verheyen, K., 2022. Forest structure and composition alleviate human thermal stress. Glob. Chang. Biol. 28, 7340–7352. https://doi.org/10.1111/gcb.16419.
Gillerot, L., Rozario, K., de Frenne, P., Oh, R., Ponette, Q., Bonn, A., Chow, W., Godbold, D., Steinparzer, M., Haluza, D., Landuyt, D., Muys, B., Verheyen, K., 2024b. Forests are chill: The interplay between thermal comfort and mental wellbeing. Landsc. Urban Plan. 242, 13. https://doi.org/10.1016/j.landurbplan.2023.104933.
Greiser, C., Meineri, E., Luoto, M., Ehrlén, J., Hylander, K., 2018. Monthly microclimate models in a managed boreal forest landscape. Agric. For. Meteorol. 250–251, 147–158. https://doi.org/10.1016/j.agrformet.2017.12.252.
Guan, B.T., Hsu, H.W., Wey, T.H., Tsao, L.S., 2009. Modeling monthly mean temperatures for the mountain regions of Taiwan by generalized additive models. Agric. For. Meteorol. 149, 281–290. https://doi.org/10.1016/j.agrformet.2008.08.010.
Haesen, S., Lembrechts, J.J., De Frenne, P., Lenoir, J., Aalto, J., Ashcroft, M.B., Kopecký, M., Luoto, M., Maclean, I., Nijs, I., Niittynen, P., van den Hoogen, J., Arriga, N., Brůna, J., Buchmann, N., Čiliak, M., Collalti, A., De Lombaerde, E., Descombes, P., Gharun, M., Goded, I., Govaert, S., Greiser, C., Grelle, A., Gruening, C., Hederová, L., Hylander, K., Kreyling, J., Kruijt, B., Macek, M., Máliš, F., Man, M., Manca, G., Matula, R., Meeussen, C., Merinero, S., Minerbi, S., Montagnani, L., Muffler, L., Ogaya, R., Penuelas, J., Plichta, R., Portillo-Estrada, M., Schmeddes, J., Shekhar, A., Spicher, F., Ujházyová, M., Vangansbeke, P., Weigel, R., Wild, J., Zellweger, F., Van Meerbeek, K., 2021. ForestTemp – Sub-canopy microclimate temperatures of European forests. Glob. Chang. Biol. 27, 6307–6319. https://doi.org/10.1111/gcb.15892.
Haesen, S., Lembrechts, J.J., Frenne, P., De, Lenoir, Aalto, J., Ashcroft, J., Kopecký, M.B., Luoto, M., Kreyling, M., Kruijt, J., Macek, B., Máliš, M., Estrada, F., Schmeddes, M. P.-, Shekhar, J., Spicher, A., Ujházyová, F., Vangansbeke, M., Weigel, P., Wild, R., Zellweger, J., Meerbeek, F., Van, K., 2023. ForestClim — - Bioclimatic variables for microclimate temperatures of European forests. Glob. Chang. Biol. 29, 2886–2892. https://doi.org/10.1111/gcb.16678.
Hardwick, S.R., Toumi, R., Pfeifer, M., Turner, E.C., Nilus, R., Ewers, R.M., 2015. The relationship between leaf area index and microclimate in tropical forest and oil palm plantation: Forest disturbance drives changes in microclimate. Agric. For. Meteorol. 201, 187–195. https://doi.org/10.1016/j.agrformet.2014.11.010.
Hastie, T.J., Tibshirani, R., 1986. Generalized additive models. Stat. Sci. 1, 297–318. https://doi.org/10.1201/9780203738535.
Hutchison, B.A., Matt, D.R., 1977. The Distribution of Solar Radiation within a Deciduous Forest. Eol. Monogr. 47, 185–207.
ISO, 1998. ISO 7726:1998 Ergonomics of the thermal environment Instruments for measuring physical quantities.
Johansson, E., Thorsson, S., Emmanuel, R., Krüger, E., 2014. Instruments and methods in outdoor thermal comfort studies - The need for standardization. Urban Clim. 10, 346–366. https://doi.org/10.1016/j.uclim.2013.12.002.
Jucker, T., Bouriaud, O., Coomes, D.A., 2015. Crown plasticity enables trees to optimize canopy packing in mixed-species forests. Funct. Ecol. 29, 1078–1086. https://doi.org/10.1111/1365-2435.12428.
Jucker, T., Hardwick, S.R., Both, S., Elias, D.M.O., Ewers, R.M., Milodowski, D.T., Swinfield, T., Coomes, D.A., 2018. Canopy structure and topography jointly constrain the microclimate of human-modified tropical landscapes. Glob. Chang. Biol. 24, 5243–5258. https://doi.org/10.1111/gcb.14415.
Koenig, W.D., Knops, J.M.H., Carmen, W.J., Pearse, I.S., 2015. What drives masting? The phenological synchrony hypothesis. Ecology 96, 184–192. https://doi.org/10.1890/14-0819.1.
Koenig, W.D., Knops, J.M.H., Pesendorfer, M.B., Zaya, D.N., Ashley, M.V., 2017. Drivers of synchrony of acorn production in the valley oak (Quercus lobata) at two spatial scales. Ecology 98, 3056–3062. https://doi.org/10.1002/ecy.2010.
Kotzen, B., 2003. An investigation of shade under six different tree species of the Negev desert towards their potential use for enhancing micro-climatic conditions in landscape architectural development. J. Arid Environ. 55, 231–274. https://doi.org/10.1016/S0140-1963(03)00030-2.
Kovács, B., Tinya, F., Ódor, P., 2017. Stand structural drivers of microclimate in mature temperate mixed forests. Agric. For. Meteorol. 234–235, 11–21. https://doi.org/10.1016/j.agrformet.2016.11.268.
Laanaya, F., St-Hilaire, A., Gloaguen, E., 2017. Water temperature modelling: comparison between the generalized additive model, logistic, residuals regression and linear regression models. Hydrol. Sci. J. 62, 1078–1093. https://doi.org/10.1080/02626667.2016.1246799.
Lai, J., Tang, J., Li, T., Zhang, A., Mao, L., 2024. Evaluating the relative importance of predictors in Generalized Additive Models using the gam.hp R package. Plant Divers 46, 542–546. https://doi.org/10.1016/j.pld.2024.06.002.
Leuzinger, S., Körner, C., 2007. Tree species diversity affects canopy leaf temperatures in a mature temperate forest. Agric. For. Meteorol. 146, 29–37. https://doi.org/10.1016/j.agrformet.2007.05.007.
Liang, J., Crowther, T.W., Picard, N., Wiser, S., Zhou, M., Alberti, G., Schulze, E.D., McGuire, A.D., Bozzato, F., Pretzsch, H., De-Miguel, S., Paquette, A., Hérault, B., Scherer-Lorenzen, M., Barrett, C.B., Glick, H.B., Hengeveld, G.M., Nabuurs, G.J., Pfautsch, S., Viana, H., Vibrans, A.C., Ammer, C., Schall, P., Verbyla, D., Tchebakova, N., Fischer, M., Watson, J.V., Chen, H.Y.H., Lei, X., Schelhaas, M.J., Lu, H., Gianelle, D., Parfenova, E.I., Salas, C., Lee, E., Lee, B., Kim, H.S., Bruelheide, H., Coomes, D.A., Piotto, D., Sunderland, T., Schmid, B., Gourlet-Fleury, S., Sonké, B., Tavani, R., Zhu, J., Brandl, S., Vayreda, J., Kitahara, F., Searle, E.B., Neldner, V.J., Ngugi, M.R., Baraloto, C., Frizzera, L., Bałazy, R., Oleksyn, J., Zawiła-Niedźwiecki, T., Bouriaud, O., Bussotti, F., Finér, L., Jaroszewicz, B., Jucker, T., Valladares, F., Jagodzinski, A.M., Peri, P.L., Gonmadje, C., Marthy, W., O'Brien, T., Martin, E.H., Marshall, A.R., Rovero, F., Bitariho, R., Niklaus, P.A., Alvarez-Loayza, P., Chamuya, N., Valencia, R., Mortier, F., Wortel, V., Engone-Obiang, N.L., Ferreira, L.V., Odeke, D.E., Vasquez, R. M., Lewis, S.L., Reich, P.B., 2016. Positive biodiversity-productivity relationship predominant in global forests. Science 354 (80), aaf8957. https://doi.org/10.1126/science.aaf8957.
Lindenmayer, D., Blanchard, W., McBurney, L., Bowd, E., Youngentob, K., Marsh, K., Taylor, C., 2022. Stand age related differences in forest microclimate. For. Ecol. Manag. 510, 120101. https://doi.org/10.1016/j.foreco.2022.120101.
Lundquist, J.D., Huggett, B., 2008. Evergreen trees as inexpensive radiation shields for temperature sensors. Water Resour. Res. 46, 1–5. https://doi.org/10.1029/2008WR006979.
Maclean, I.M.D., Duffy, J.P., Haesen, S., Govaert, S., De Frenne, P., Vanneste, T., Lenoir, J., Lembrechts, J.J., Rhodes, M.W., Van Meerbeek, K., 2021a. On the measurement of microclimate. Methods Ecol. Evol. 12, 1397–1410. https://doi.org/10.1111/2041-210X.13627.

Maclean, I.M.D., Klinges, H.K., Klinges, D.H., Klinges, H.K., 2021b. Microclimc: A mechanistic model of above, below and within-canopy microclimate. Ecol. Modell. 451, 109567. https://doi.org/10.1016/j.ecolmodel.2021.109567.
Marra, G., Wood, S.N., 2011. Practical variable selection for generalized additive models. Comput. Stat. Data Anal. 55, 2372–2387. https://doi.org/10.1016/j.csda.2011.02.004.
Meili, N., Manoli, G., Burlando, P., Carmeliet, J., Chow, W.T.L., Coutts, A.M., Roth, M., Velasco, E., Vivoni, E.R., Fatichi, S., 2021. Tree effects on urban microclimate: Diurnal, seasonal, and climatic temperature differences explained by separating radiation, evapotranspiration, and roughness effects. Urban For. Urban Green. 58, 126970. https://doi.org/10.1016/j.ufug.2020.126970.
Morin, X., Fahse, L., Scherer-Lorenzen, M., Bugmann, H., 2011. Tree species richness promotes productivity in temperate forests through strong complementarity between species. Ecol. Lett. 14, 1211–1219. https://doi.org/10.1111/j.1461-0248.2011.01691.x.
Owusu, G., 2023. The Surface Energy Balance and Crop Coefficient Estimation with R [WWW Document]. URL ⟨https://rdrr.io/github/gowusu/sebkc/man/ETohr.html⟩ (accessed 6.1.23).
Pedersen, E.J., Miller, D.L., Simpson, G.L., Ross, N., 2019. Hierarchical generalized additive models in ecology: An introduction with mgcv. PeerJ 2019. https://doi.org/10.7717/peerj.6876.
Pretzsch, H., 2014. Canopy space filling and tree crown morphology in mixed-species stands compared with monocultures. For. Ecol. Manag. 327, 251–264. https://doi.org/10.1016/j.foreco.2014.04.027.
Pretzsch, H., 2019. Grundlagen der Waldwachstumsforschung. Springer-Verlag, Freising, Germany.
Pretzsch, H., del Río, M., Schütze, G., Ammer, C., Annighöfer, P., Avdagic, A., Barbeito, I., Bielak, K., Brazaitis, G., Coll, L., Drössler, L., Fabrika, M., Forrester, D.I., Kurylyak, V., Löf, M., Lombardi, F., Matović, B., Mohren, F., Motta, R., den Ouden, J., Pach, M., Ponette, Q., Skrzyszewski, J., Sramek, V., Sterba, H., Svoboda, M., Verheyen, K., Zlatanov, T., Bravo-Oviedo, A., 2016. Mixing of Scots pine (Pinus sylvestris L.) and European beech (Fagus sylvatica L.) enhances structural heterogeneity, And the effect increases with water availability. For. Ecol. Manag. 373, 149–166. https://doi.org/10.1016/j.foreco.2016.04.043.
Pretzsch, H., Schütze, G., 2016. Effect of tree species mixing on the size structure, density, and yield of forest stands. Eur. J. For. Res. 135, 1–22. https://doi.org/10.1007/s10342-015-0913-z.
Quadri, P., Silva, L.C.R., Zavaleta, E.S., 2021. Climate-induced reversal of tree growth patterns at a tropical treeline. Sci. Adv. 7. https://doi.org/10.1126/sciadv.abb7572.
Rahman, M.A., Stratopoulos, L.M.F., Moser-Reischl, A., Zölch, T., Häberle, K.H., Rötzer, T., Pretzsch, H., Pauleit, S., 2020. Traits of trees for cooling urban heat islands: A meta-analysis. Build. Environ. 170. https://doi.org/10.1016/j.buildenv.2019.106606.
Raupach, M.R., Finnigan, J.J., Brunet, Y., 1996. Coherent Eddies And Turbulence In Vegetation Canopies: The Mixing-Layer Analogy. Bound. -Layer. Meteor. 78, 351–382.
Renaud, V., Innes, J.L., Dobbertin, M., Rebetez, M., 2011. Comparison between open-site and below-canopy climatic conditions in Switzerland for different types of forests over 10 years (1998-2007). Theor. Appl. Climatol. 105, 119–127. https://doi.org/10.1007/s00704-010-0361-0.
Renaud, V., Rebetez, M., 2009. Comparison between open-site and below-canopy climatic conditions in Switzerland during the exceptionally hot summer of 2003. Agric. For. Meteorol. 149, 873–880. https://doi.org/10.1016/j.agrformet.2008.11.006.
del Río, M., Vergarechea, M., Hilmers, T., Alday, J.G., Avdagić, A., Binderh, F., Bosela, M., Dobor, L., Forrester, D.I., Halilović, V., Ibrahimspahić, A., Klopcic, M., Lévesque, M., Nagel, T.A., Sitkova, Z., Schütze, G., Stajić, B., Stojanović, D., Uhl, E., Zlatanov, T., Tognetti, R., Pretzsch, H., 2021. Effects of elevation-dependent climate warming on intra- and inter-specific growth synchrony in mixed mountain forests. For. Ecol. Manag. 479, 118587. https://doi.org/10.1016/j.foreco.2020.118587.
Royer, P.D., Cobb, N.S., Clifford, M.J., Huang, C.Y., Breshears, D.D., Adams, H.D., Villegas, J.C., 2011. Extreme climatic event-triggered overstorey vegetation loss increases understorey solar input regionally: Primary and secondary ecological implications. J. Ecol. 99, 714–723. https://doi.org/10.1111/j.1365-2745.2011.01804.x.
Roznik, E.A., Alford, R.A., 2012. Does waterproofing Thermochron iButton dataloggers influence temperature readings? J. Therm. Biol. 37, 260–264. https://doi.org/10.1016/j.jtherbio.2012.02.004.
Sanczuk, P., Pauw, K., De, Lombaerde, De, E., Luoto, M., Meeussen, C., Govaert, S., Vanneste, T., Depauw, L., Brunet, J., Cousins, S.A.O., Gasperini, C., Hedwall, P., Iacopetti, G., Lenoir, J., Plue, J., Selvi, F., Spicher, F., Uria-diez, J., Verheyen, K., Vangansbeke, P., Frenne, P., De, 2023. Microclimate and forest density drive plant population dynamics under climate change. Nat. Clim. Chang. 13. https://doi.org/10.1038/s41558-023-01744-y.
Schnabel, F., Beugnon, R., Yang, B., Richter, R., Eisenhauer, N., 2024. Tree diversity increases forest temperature buffering. bioRxiv. https://doi.org/10.1101/2023.09.11.556807.
Shahidan, M.F., Shariff, M.K.M., Jones, P., Salleh, E., Abdullah, A.M., 2010. A comparison of Mesua ferrea L. and Hura crepitans L. for shade creation and radiation modification in improving thermal comfort. Landsc. Urban Plan. 97, 168–181. https://doi.org/10.1016/j.landurbplan.2010.05.008.
Simpson, G.L., 2018. Modelling palaeoecological time series using generalised additive models. Front. Ecol. Evol. 6, 1–21. https://doi.org/10.3389/fevo.2018.00149.
Staines, M.N., Booth, D.T., Laloë, J.O., Tibbetts, I.R., Hays, G.C., 2022. The ecological importance of the accuracy of environmental temperature measurements. Biol. Lett. 18, 6. https://doi.org/10.1098/rsbl.2022.0263.
Steinparzer, M., Haluza, D., Godbold, D.L., 2022. Integrating Tree Species Identity and Diversity in Particulate Matter Adsorption. Forests 13, 1–15. https://doi.org/10.3390/f13030481.
Strieder, E., Vospernik, S., 2021. Intra-annual diameter growth variation of six common european tree species in pure and mixed stands. Silva Fenn. 55, 1–29. https://doi.org/10.14214/SF.10449.
Terando, A.J., Youngsteadt, E., Meineke, E.K., Prado, S.G., 2017. Ad hoc instrumentation methods in ecological studies produce highly biased temperature measurements. Ecol. Evol. 7, 9890–9904. https://doi.org/10.1002/ece3.3499.
Thoen, E., 2022. _padr: Quickly Get Datetime Data Ready for Analysis_. R package version 0.6.2. ⟨https://cran.r-project.org/package=padr⟩.
Upreti, R., Wang, Z.H., Yang, J., 2017. Radiative shading effect of urban trees on cooling the regional built environment. Urban For. Urban Green. 26, 18–24. https://doi.org/10.1016/j.ufug.2017.05.008.
Urgoiti, J., Messier, C., Keeton, W.S., Reich, P.B., Gravel, D., Paquette, A., 2022. No complementarity no gain—Net diversity effects on tree productivity occur once complementarity emerges during early stand development. Ecol. Lett. 25, 851–862. https://doi.org/10.1111/ele.13959.
van de Pol, M., Bailey, L.D., McLean, N., Rijsdijk, L., Lawson, C.R., Brouwer, L., 2016. Identifying the best climatic predictors in ecology and evolution. Methods Ecol. Evol. 7, 1246–1257. https://doi.org/10.1111/2041-210X.12590.
Verheyen, K., Vanhellemont, M., Auge, H., Baeten, L., Baraloto, C., Barsoum, N., Bilodeau-Gauthier, S., Bruelheide, H., Castagneyrol, B., Godbold, D., Haase, J., Hector, A., Jactel, H., Koricheva, J., Loreau, M., Mereu, S., Messier, C., Muys, B., Nolet, P., Paquette, A., Parker, J., Perring, M., Ponette, Q., Potvin, C., Reich, P., Smith, A., Weih, M., Scherer-Lorenzen, M., 2016. Contributions of a global network of tree diversity experiments to sustainable forest plantations. Ambio 45, 29–41. https://doi.org/10.1007/s13280-015-0685-1.
Von Arx, G., Dobbertin, M., Rebetez, M., 2012. Spatio-temporal effects of forest canopy on understory microclimate in a long-term experiment in Switzerland. Agric. For. Meteorol. 166–167, 144–155. https://doi.org/10.1016/j.agrformet.2012.07.018.
Von Arx, G., Graf Pannatier, E., Thimonier, A., Rebetez, M., 2013. Microclimate in forests with varying leaf area index and soil moisture: Potential implications for seedling establishment in a changing climate. J. Ecol. 101, 1201–1213. https://doi.org/10.1111/1365-2745.12121.
Vospernik, S., 2021. Basal area increment models accounting for climate and mixture for Austrian tree species. For. Ecol. Manag. 480. https://doi.org/10.1016/j.foreco.2020.118725.
Vospernik, S., Heym, M., Pretzsch, H., Pach, M., Steckel, M., Del, M., Magnus, L., Pardos, M., Bielak, K., Bravo, F., Coll, L., Cerný, J., Droessler, L., Ehbrecht, M., Jansons, A., Korboulewsky, N., Jourdan, M., Nord-larsen, T., Nothdurft, A., Ruiz-peinado, R., Ponette, Q., Sitko, R., Svoboda, M., Wolff, B., 2023. Tree species growth response to climate in mixtures of Quercus robur/Quercus petraea and Pinus sylvestris across Europe - a dynamic, sensitive equilibrium. For. Ecol. Manag. 530, 15. https://doi.org/10.1016/j.foreco.2022.120753.
Wang, X., Dallimer, M., Scott, C.E., Shi, W., Gao, J., 2021. Tree species richness and diversity predicts the magnitude of urban heat island mitigation effects of greenspaces. Sci. Total Environ. 770, 145211. https://doi.org/10.1016/j.scitotenv.2021.145211.
Werner, R., Gasser, L.T., Steinparzer, M., Mayer, M., Ahmed, I.U., Sandén, H., Godbold, D.L., Rewald, B., 2024. Early overyielding in a mixed deciduous forest is driven by both above- and below-ground species-specific acclimatization. Ann. Bot. 134, 1077–1095. https://doi.org/10.1093/aob/mcae150.
Wesołowski, T., Rowiński, P., 2006. Timing of bud burst and tree-leaf development in a multispecies temperate forest. For. Ecol. Manag. 237, 387–393. https://doi.org/10.1016/j.foreco.2006.09.061.
Wood, S.N., 2003. Thin plate regression splines. J. R. Stat. Soc. Ser. B Stat. Methodol. 65, 95–114. https://doi.org/10.1111/1467-9868.00374.
Wood, S.N., 2011. Fast stable restricted maximum likelihood and marginal likelihood estimation of semiparametric generalized linear models. J. R. Stat. Soc. Ser. B Stat. Methodol. 73, 3–36. https://doi.org/10.1111/j.1467-9868.2010.00749.x.
Wood, S.N., 2017. Generalized Additive Models - An Introduction with R, Second Edi. ed. CRC Press Taylor & Francis Group, A Chapman & Hall Book, Boca Raton.
Wood, S.N., Goude, Y., Shaw, S., 2015. Generalized additive models for large data sets. J. R. Stat. Soc. Ser. C. Appl. Stat. 64, 139–155. https://doi.org/10.1111/rssc.12068.
Wood, S.N., Pya, N., Säfken, B., 2016. Smoothing Parameter and Model Selection for General Smooth Models. J. Am. Stat. Assoc. 111, 1548–1563. https://doi.org/10.1080/01621459.2016.1180986.
ZAMG, 2002. Klimadaten von Österreich 1971 - 2000 [WWW Document]. URL ⟨https://www.zamg.ac.at/fix/klima/oe71-00/klima2000/klimadaten_oesterreich_1971_frame1.htm⟩ (accessed 6.1.23).
ZAMG, 2019. Beobachtungsanleitung für die Phänologie. Vienna.
Zellweger, F., Coomes, D., Lenoir, J., Depauw, L., Maes, S.L., Wulf, M., Kirby, K.J., Brunet, J., Kopecký, M., Máliš, F., Schmidt, W., Heinrichs, S., den Ouden, J., Jaroszewicz, B., Buyse, G., Spicher, F., Verheyen, K., De Frenne, P., 2019. Seasonal drivers of understorey temperature buffering in temperate deciduous forests across Europe. Glob. Ecol. Biogeogr. 28, 1774–1786. https://doi.org/10.1111/geb.12991.
Zellweger, F., De Frenne, P., Lenoir, J., Vangansbeke, P., Verheyen, K., Bernhardt-römermann, M., Baeten, L., Hédl, R., Berki, I., Brunet, J., Van Calster, H., Chudomelov, 2020. Forest microclimate dynamics drive plant responses to warming. Science 368 (80), 772–775. https://doi.org/10.1126/science.aba6880.
Zhang, S., Landuyt, D., Verheyen, K., De Frenne, P., 2022. Tree species mixing can amplify microclimate offsets in young forest plantations. J. Appl. Ecol. 59, 1428–1439. https://doi.org/10.1111/1365-2664.14158.